Research Report 2016-11

# Diagnostics of the multi-model ensemble seasonal forecast of the APEC Climate Center: Forecast skill and predictability of ENSO and its response

Soo-Jin Sohn

APEC CLIMATE CENTER

Research Report 2016-11

# Diagnostics of the multi-model ensemble seasonal forecast of the APEC Climate Center: Forecast skill and predictability of ENSO and its response

Soo-Jin Sohn

APCC
APEC CLIMATE CENTER

# PREFACE

The El Niño-Southern Oscillation (ENSO), one of the most important climate drivers, greatly influences climate in both the Tropics and remote regions. As such ENSO can play the role of a main predictability source in regional climate forecasts. Because of their importance, the ENSO phenomenon and global sea surface temperature (SST) changes are constantly being monitored by most operational centers. Some of them, including the Japan Meteorological Administration (JMA), International Research Institute of Climate and Society (IRI), National Centers for Environmental Prediction (NCEP), Korean Meteorological Administration (KMA), Australian Government Bureau of Meteorology (BOM), APEC Climate Center (APCC), and others, provide forecasts of ENSO evolution and the associated climate anomalies. Although numerous studies on the predictability of ENSO and its climate impacts have been conducted, the possible roles of the intensity and the flavor of ENSO on SST predictions are still not well established.

Based on the APCC Tier-1 multi-model ensemble (MME) hindcast experiments, how the amplitude and flavor of ENSO might affect SST predictability has been assessed. The prediction skill and predictability of conventional ENSO and its diversity have been also examined. These study results give us the following broad implications. First, a good ENSO forecast (based on only the Niño 3.4 index) cannot guarantee a good SST prediction. The strength, as well as the flavor of ENSO, needs to be considered when interpreting SST and other products from dynamical seasonal prediction systems. Next, it is quite important to know the upper limit of predictability and the actual prediction skill of ENSO diversity, which can provide room for model improvement and better understanding of ENSO prediction. These results shed light on the challenging problem of changes in ENSO and diversity-related predictability.

Finally, I would like to express my gratitude to Dr. Soo-Jin Sohn and the other collaborators for their dedication and efforts to successfully complete this study.

Dr. **Hong-Sang Jung**
President, APEC Climate Center
January 2017

# ABSTRACT

The effect of the amplitude and type of the El Niño-Southern Oscillation (ENSO) on the sea surface temperature (SST) predictability has been assessed through Asia-Pacific Economic Cooperation (APEC) Climate Center (APCC) Tier-1 multi-model ensemble (MME) hindcast experiments. The forecast skill and predictability of the conventional ENSO and its diversity were also examined. The MME predicts the Niño3.4 index well, even at a 4-month lead time. However, capturing the SST pattern during weak ENSO events is difficult. All weak El Niños were found to be El Niño Modoki. Some models fail to reproduce the associated tripole SST pattern over the tropical Pacific. The SST signals of the MME are less persistent than the temperature observed during weak La Niña periods.

The leading modes and residuals of the tropical Pacific SST variability were identified based on the empirical orthogonal function (EOF) analysis of monthly values. The first forced mode and its residual indicate the canonical ENSO-related and ENSO diversity-related variability, respectively. The forecast skill of the conventional ENSO remains significant up to a 6-month lead time. The ability to predict ENSO diversity is limited and has a shorter lead time. In addition, the variance of ENSO diversity is relatively smaller than that of the canonical ENSO-related variability. The potential predictability of the ENSO diversity was also investigated to reveal the signal factor of the types. The predictability source was determined for the entire tropical Pacific; the predictability appears to be stable at long lead times.

These results have the following broad implications. First, a good ENSO forecast-

based only on the Niño3.4 index cannot guarantee a good SST prediction. The strength and type of the ENSO needs to be considered when interpreting SST and other products of dynamical seasonal prediction systems. Second, it is important to know the upper limit of the predictability and actual forecast skill of the ENSO diversity, which helps to improve the model and better understand the ENSO prediction. The results shed light on the challenging problem of ENSO changes and the diversity-related predictability.

# CONTENTS

# 1. INTRODUCTION

Seasonal climate prediction using dynamical general circulation models (GCMs) has been drastically improved during recent decades (Goddard et al. 2001) with the advancement of climate observation and modeling systems and initialization and assimilation technology as well as better knowledge and best practice in climate forecasting (Wang et al. 2009). The post-processing, such as calibration and combination, has also contributed to the improved performance of dynamical seasonal climate predictions (Coelho et al. 2004; Doblas-Reyes et al. 2005). It is known, for instance, that multi-model ensemble (MME) systems combing several dynamical climate models can improve the seasonal forecasts by reducing systematic errors and random noise (Yoo and Kang 2005).

The better understanding of the El Niño-Southern Oscillation (ENSO) is another key factor for good seasonal and interannual climate predictions; tropical oceanic and atmospheric processes and sea surface temperatures (SSTs) drive the predictable part of the climate as surface boundary conditions. The ENSO forecast skill improved due to the advanced capability of state-of-the-art coupled atmosphere and ocean general circulation models (CCGMs or AOGCMs; e.g., Guilyardi et al. 2009). The current ENSO prediction skill in dynamical seasonal forecasting exceeds that of statistical forecasting; the capability of ENSO forecasts is increasing (Barnston et al. 2012).

The potential predictability (PP) is used in various applications from weather to climate forecasting to describe the future condition prediction extent in principle, which means it describes the proportion of the variance due to systematic factors rather than random noise. The systematic factors and random noise can be differentiated from the forecasted targeted time scales (Waliser et al. 2003; Ajaya Mohan and Goswami 2003; Boer 2011). In general, the potential seasonal predictability is identified based on the difference between the actual and weather noise-induced variability (DelSole et al. 2013), which can be estimated from the signal-to-noise ratio of the total variance with a certain prediction model ensemble or system (Rowell 1998; Phelps et al. 2004). Fast and small-scale processes, such as the weather itself (e.g., tropical cyclones), characterize the noise part in seasonal climate predictions. On the other hand, the signal part indicates slowly varying large-scale processes such as SST, soil moisture, and sea ice as external forcing. Phenomena representative for the signal are the ENSO or Intertropical Convergence Zone (ITCZ). Although current dynamical prediction models and systems have difficulties to properly predict a relevant precipitation band due to the double ITCZ problem (Li and Xie 2014) and cold tongue bias in the tropical Pacific (Luo et al. 2005; Misra et al. 2008), they at least predict ENSO at a 6-month lead time in seasonal climate forecasting well (Jin et al. 2008; Wang et al. 2009; Barnston et al. 2012; Imada et al. 2015).

The ENSO is one of the most important climate drivers (Lau 1997; Rasmusson and Wallace 1983; Ropelewski and Halpert 1987, 1996; Trenberth and Caron 2000) and greatly influences the climate in both the tropics and remote regions (Zhang et al. 1997; Chen et al. 2000; Lau and Wang 2005; Wang et al. 2000, 2008; Weng et al. 2009). Therefore, ENSO plays a role as main predictability source in regional climate forecasts (Larkin and Harrison 2005). In fact, many seasonal prediction schemes are constructed based on SST information (Colman and Davey 2003) due to its important role in inciting low-frequency atmospheric changes (Lau 1997; Shukla et al. 2000). For instance, skillful forecasts of the Indian summer monsoon rainfall can be obtained based on the global SST evolution at long lead times (Sahai et al. 2003). Some studies also reported that anomalous SSTs of regional seas influence the climate variability in local areas (Goddard and Graham 1999; Meehl and Arblaster 2002; Behera et al. 2005; Zhou et al. 2010). It is clear that SST is a key parameter in considering seasonal and interannual climate variations (Kug et al. 2007).

Because of their importance, the ENSO phenomenon and global SST changes are constantly being monitored by most operational centers. Several of these centers, including the Japan Meteorological Administration (JMA), International Research Institute of Climate and Society (IRI), National Centers for Environmental Prediction (NCEP), Korean Meteorological Administration (KMA), Australian Government Bureau of Meteorology (BOM), and APEC Climate Center (APCC), even provide forecasts of their evolution and associated climate anomalies. Although numerous studies on the predictability of ENSO and its climate impact have been conducted, the possible roles of the intensity and type of ENSO on SST predictions are still not well established. Jin et al. (2008) evaluated the ENSO prediction skill in atmosphere-ocean coupled models and found that it is higher during El Niño/La Niña events than in normal periods.

The change of the climate system has modulated the frequencies and characteristics of tropical Indo-Pacific climate phenomena and consequently their global impact since the late 1970s (Ashok et al. 2007). Recently, a new ENSO type different from the canonical type (Rasmusson and Carpenter 1982; Trenberth 1997) has been discovered (Ashok and Yamagata 2009). It is known as dateline El Niño, ENSO Modoki, and is a central-Pacific ENSO type or warm pool (WP) El Niño. Anomalous SST warming over the central Pacific rather than the far eastern Pacific characterize its warm phase (Lakin and Harrison 2005; Ashok et al. 2007; Yu and Kao 2007; Kao and Yu 2009; Kug et al. 2009, 2010). The cold phase of the atypical El Niño is still debated; it is less distinctive due to the strong El Niño-La Niña asymmetry (Kug and Ham 2011), which sometimes is identified as the linear counterpart of the atypical El Niño (Cai and Cowan 2009; Yuan and Yan 2013). The climate impact of ENSO Modoki also differs from that of typical canonical ENSO events (Ashok et al. 2007; Weng et al. 2009; Chen and Tam 2010; Feng et al. 2011, 2006; Cai and Cowan 2009; Kaori et al. 2013; Infanti and Kirtman 2016).

Several efforts have been made to identify the two types of El Niño events and to isolate them from each other (Yu et al. 2012). Those methods are usually based on an index-based definition, such as the Niño3 and Niño4 indices (Yuan and Yan 2013) and their combinations and the El Niño Modoki index (EMI; Ahosk et al. 2007), or dualistic definition with empirical orthogonal function (EOF) separation. To measure the different responses of the atmospheric circulation to the two types of El Niño, the related two southern oscillation indices are defined based on the air-sea coupled relationship between the eddy sea lever pressure and SST (Xu et al. 2013). The ability of climate models to simulate ENSO and its dynamical seasonal prediction variance has been assessed based on aforementioned definitions (Imada et al. 2015). The response of the North American rainfall and temperature prediction to the two types of El Niño events has been investigated using the consensus method from Yu et al. (2012) based on the North American MME (NMME) system (Infanti and Kirtman 2016). However, none of the studies focused on the dependence of the ENSO predictability on its strengths and types in coupled models. The influence of such factors on the ENSO diversity needs to be assessed in current coupled models because nonlinear dynamics of the ocean behavior and intrinsic internal variability are responsible for an irregular ENSO.

Therefore, the accuracy of the prediction of the ENSO strength and type and associated SST changes using coupled models is assessed in this study. We also aim to isolate the canonical ENSO, which can be used for seasonal prediction, from its diversity to search for predictable areas of the ENSO diversity in current coupled seasonal climate models. The rest of this paper is organized as follows. The datasets and methodology are described in Section 2. The ability of the climate models to predict the ENSO and global SST signals for different ENSO intensities and phases are examined in Section 3. The forecast skill of ENSO and predictability of the ENSO diversity are evaluated in Section 4. The discussion and summary can be found in Section 5.

# 2. DATASETS AND METHODOLOGY

## 2.1 DATA

Seasonal retrospective forecast experiments based on eight independent coupled climate models of the operational monthly 6-month multi-model ensemble (MME) climate outlook[1] of the APCC (Korea) were used in this study to assess the ability of ocean–atmosphere coupled models in predicting ENSO. The considered hindcasts are based on Coupled Model Intercomparison Project (CMIP)-type experiments (Covey et al. 2003). They are produced by a one-tier prediction system using a coupled AOGCM, which is based on the air–sea interaction in the prediction system; SST and ENSO predictions[2] with lead times of 6 months and beyond can be made. The acronyms of institutions and models are listed in Table 1. Table 2 presents a brief summary of the model experiments including model specifications and ensemble sizes. The individual coupled models consist of atmospheric and ocean components with different horizontal and vertical resolutions. All model simulation data were interpolated onto the same 2.5°×2.5° grid prior to any calculation or comparison. Moreover, each model has different ensemble member and hindcast periods. In contrast to previous conventional diagnostic studies using common hindcast periods, the hindcast period of each model is considered in this study (see Table 2) to diagnose the model behavior and characteristics with respect to the ENSO forecast skill and predictability and its diversity, which is based on the fact the WP-type El Niño has frequently occurred during recent periods, even after 2005 (Yu et al. 2012). The common hindcast period from 1983 to 2005 is considered for the MME mean, which is computed as the simple unweighted average of the ensemble mean forecasts of all available single coupled models (SMEs; Sohn et al. 2011).

All hindcast datasets are available from January to December and have lead times of 6 months. The models of the hindcast experiments were initiated based on the conditions observed one month prior to a particular target season. The

---

1) http://www.apcc21.org/ser/outlook.do?lang=en
2) http://www.apcc21.org/ser/enso.do?lang=en

strategies for initializing the forecast systems are briefly addressed in Table 3. For comparison, a persistent forecast is made by prescribing the initial SST anomalies (SSTAs) throughout the entire forecast period (Roads et al. 2001). For example, the observed SSTA for April is persisted for the forecast from June to November (initialized in May; Wang et al. 2009). The one-month and four-month lead prediction skills for all consecutive three-month periods of the calendar year were assessed using these datasets. In addition, the SST predictions during the boreal warm season (defined as the average of June-July-August, July-August-September, August-September-October, and September-October-November forecasts based on the initial conditions of May 1) and cold season (defined as the average of December-January-February, January-February-March, and February-March-April forecasts that were initiated on November 1) were also examined.

The observational datasets used in this study are the optimum interpolations (OI) of the SST data (Reynolds et al. 2002) and Climate Anomaly Monitoring System (CAM) and Outgoing Longwave Radiation (OLR) Precipitation Index (OPI) product (CAMS OPI; Janowiak and Xie 1999), which are employed as reference data for the operational verification of the 6-month MME climate prediction of the APCC due to the their timely update on a monthly basis. The former was used to examine the ENSO and its associated SST variability. Both datasets were interpolated onto a 2.5°×2.5° grid using the coordinates of the coupled model datasets.

## 2.2 El Niño-Southern Oscillation definition and classification

To determine the phase and amplitude of the conventional ENSO, the Niño3.4 index (defined as area average of the region of 5°S–5°N and 170°-120°W; Trenberth 1997) based on the three-month running mean SST anomalies was used. The El Niño (La Niña) events for at least four consecutive overlapping three-month periods were identified whenever the index was larger (smaller) than the standard deviation of 0.65 (-0.65; see Table 4). Among these events, the ENSO occurrences were further classified as strong or weak depending on whether the absolute magnitude of the Niño3.4 index was larger than the standard deviation of 1.3 or not. Based on these definitions, strong and weak El Niño/La Niña periods were identified (Table 5).

The El Niño Modoki events were defined as periods during which the amplitude of the El Niño Modoki index (EMI) has a standard deviation of at least 0.7 (Ashok et al. 2007). Its counterpart in the cold phase, however, appears to be less distinctive due to a strong El Niño-La Niña asymmetry (Kug and Ham 2011); therefore, La Niña Modoki events were identified whenever the absolute value of the Niño4 index was larger than that of the Niño3 index within any La Niña period (Yuan and Yan 2013). Finally, the composite method was employed to extract recurrent climate signals accompanying the ENSO occurrences. The statistical significance of the anomalies was evaluated using the Student's t-test (Krishnan et al. 2000).

## 2.3 El Niño-Southern Oscillation and its diversity

As the major signal for seasonal climate predictability, the 1st leading mode of the EOF analysis based on monthly SST anomalies indicates the canonical ENSO. The residual of the monthly SST anomalies due to the fluctuations of the 1st mode is defined as the ENSO diversity, which causes ENSO with differences. Although the conventional El Niño is indicated by the Niño3.4 index, which contains a mixture of two types of ENSO depending on its strength and type (Sohn et al. 2016), the 1st leading mode is applied in this study. The limitation of the 1st mode in representing the ENSO dynamics and nonlinearity is not considered.

## 2.4 Verification measures

The temporal correlation coefficient (TCC), anomaly pattern correlation coefficient (ACC), and root-mean-square difference (RMSD) were used to measure the prediction skills of the SME and MME mean forecasts to determine the quality of the prediction skills of the ENSO and its diversity based on the observations (Wang et al. 2009). The TCC skill is a general measure used to evaluate the similarity between two time series in climate prediction (Barnston 1994; Sohn et al. 2013). The ratio of the ocean-forced variance to total variance using the "analysis of variance" (ANOVA) was adopted as the PP to assess the potential seasonal climate predictability using the ensembles of the individual GCM simulations (Rowell 1998). It is assumed that the potential predictable component of the interannual variability is due to the same oceanic forcing because each model is forced by equal SSTs and sea-ice extents of the different initial atmospheric conditions.

# 3. SEA SURFACE TEMPERATURE PREDICTABILITY AND ITS RELATIONSHIP WITH THE TYPE AND STRENGTH OF THE EL Niño-SOUTHERN OSCILLATION

To examine the predictability of enso based on MME, the observed Niño3.4 index was first compared with its counterparts derived from the one-month and four-month lead time MME mean forecasts. Figure 1a shows the three-month running mean results for all seasons. Overall, both one- and four-month lead time MME predictions capture the SST variability over the Niño3.4 region; the former (latter) has a temporal correlation of 0.95 (0.88) with the observation. On the other hand, there are periods during which the model results considerably deviate from the observed Niño3.4 index, especially with respect to the four-month lead MME forecasts, for example, from 1984-86 when the Niño3.4 SST is colder than normal and from 1990-1996 when an anomalously warm SST tends to persist. Interestingly, the SST signals are not strong in both of these periods, which indicates a possible relationship between the strength of the ENSO and SST predictability of the models.

Figure 1b gives the global SST prediction skill from MME, computed based on the pattern correlation between model and observed SST, as well as the absolute magnitude of the observed Niño3.4 index. From 1982 to 2006, the SST forecast skill is significantly correlated with the strength of ENSO (with correlation of 0.62). High skills are found during strong El Niño events of 1982/83, 1987/88 and 1997/98. By removing biennial signals in these timeseries, it is clear that models' skill is strongly correlated with the ENSO amplitude (with correlation of 0.85). When the amplitude of the Niño3.4 index is large, MME gives better predictions of the SST pattern over the whole globe; on the other hand, the skill score of global SST forecasts tends to be weaker during the epochs of 1984-86, the early to mid 1990's, as well as from 2001 to 2005 when the ENSO signal is weaker.

With respect to the possible impact of the ENSO amplitude on the SST predictability, the ENSO events have been classified based on the magnitude of the Niño3.4 index, as outlined in Section 3. Three out of the four strong events of the warm ENSO phase correspond to the canonical El Niño, whereas all four weak events can be classified as El Niño Modoki within period from 1982-2006 (Tables 2 and

3). Figure 2 shows the corresponding SST composites in the boreal warm season. During a strong El Niño, positive and negative anomalies are found within the deep tropical Pacific from the dateline to the South American Coast and over the western equatorial Pacific, respectively (Figure 2a). The SST is higher than normal over the Niño3.4 region; this SST pattern is apparently associated with the canonical El Niño. In comparison, weak El Niño events are characterized by an anomalously warm central equatorial Pacific, bounded by cooler regions in the west and east (Figure 2b). Such a tripole SST pattern is reminiscent of that associated with El Niño Modoki (Ashok et al. 2007). The observed SST data was first regressed onto the Niño3 and El Niño Modoki indices to quantify the degree of resemblance between these composites and those related to the two types of El Niño (see Figure 3). The pattern correlation coefficient between the canonical El Niño (El Niño Modoki) SST regression map and the aforementioned strong (weak) El Niño SST composite was determined to be 0.89 (0.71; see also Figure 4 for similar results in the boreal cold season). It is apparent that a strong (weak) warm El Niño mainly corresponds to a canonical El Niño (El Niño Modoki).

In contrast to the El Niño cases, it is noteworthy that only two out of five weak La Niña events correspond to La Niña Modoki. During strong La Niña years, the SST is lower than normal across the equatorial eastern-central Pacific. However, the anomalous SST along the equatorial Pacific in weak La Niña periods does not exhibit a tripole-like (i.e., warm-cold-warm) pattern. Also, notice that a significantly high SST is present in the northwestern Pacific during strong La Niña events, whereas for the SST signals are low during weak La Niña events in the same region. The correlation coefficient between the strong (weak) La Niña SST and the SST regression map based on the Niño3 (El Niño Modoki) index is only -0.6 (-0.38); it is clear that the SST features associated with strong and weak La Niña events are not always exact mirror images of their El Niño counterparts (see Figures A1 and A2 for another climate variability of the classified ENSO occurrences for boreal warm and cold seasons, respectively).

The model-simulated SST patterns for strong and weak ENSO events were examined. In general, the SST anomalies during strong ENSO events from all considered climate models compare well with their observational counterparts (figures not shown). On the other hand, some models seem to have difficulties in reproducing the SST patterns associated with weak ENSO events. Figure 5 shows the SST composites from the individual models and their MME mean for a weak El Niño event in the boreal warm season. During weak El Niño years, all models capture the high SST signals typically found in the central equatorial Pacific. As mentioned before, the related SST pattern greatly resembles that during El Niño Modoki; the anomalously cool regions in both the western and eastern Pacific are not well captured by some models. The models also tend to show weaker cold anomalies than the observation in the cold season over the eastern equatorial Pacific during weak El Niños (Figure 6).

To further assess the SST predictability and its relationship with the ENSO strength, the skills of the Niño3.4 index and SST pattern forecasts for each categorized ENSO event and both boreal summer and winter were compared (Figure 7). In general, the coupled models have a high fidelity in predicting the time variation of the central to eastern tropical Pacific SST. The SST forecast skills during warm and cold seasons are comparable based on the data for all years (see solid dots in Figures 7a and b); there is also evidence that the Niño3.4 index can be better predicted in boreal winter than in summer during El Niño. Consistent with our previous results, the SST tends to be more predictable during strong ENSO events than during weak events. A particularly low skill in predicting the Niño3.4 index is found in weak La Niña years, with a low temporal correlation coefficient between the MME and observations of 0.2; the correlation coefficient is ~ 0.7 to 0.8 during strong La Niña years. The analysis of the SST maps indicates that the model tends to provide less persistent signals for 1985–1986, 1995–1996, and 2000–2001 (Figure 8); this might be the reason why MME performs poorly in these weak La Niña years. The background of the cold event is more favorable for noise to provoke the ENSO cycle (An and Jin 2004; An and Wang 2005), which may prevent coupled models from simulating the ENSO cycle and evolution during weak La Niña years well.

The strength of the ENSO events is even more crucial for the determination of the model skills in capturing the accompanying global SST patterns. The global SST is well forecasted during strong El Niño years (with pattern correlations between model and observations of up to 0.66); on the other hand, this is not the case for weak El Niño years (with pattern correlations of ~0.34 to 0.5). This is consistent with our previous results regarding strong and weak El Niño SST forecasts (Figure 5). The global SST was predicted well when La Niña was strong (with pattern correlations of ~0.6 to 0.7) but when it was weak (with pattern correlations of ~0.35 to 0.5). The analysis of the individual models reveals the same tendency; the model skills in capturing global SST appear to be higher (lower) for strong (weak) ENSO events (Figure 9).

# 4. FORECAST SKILL AND PREDICTABILITY OF THE EL Niño-SOUTHERN OSCILLATION DIVERSITY

## 4.1 CONVENTIONAL EL Niño-SOUTHERN OSCILLATION FORECAST SKILLS

First of all, the conventional ENSO prediction skill was evaluated because it is the core of seasonal forecasting as major signal mode of dynamical models. Figure 10 shows the monthly mean Niño3.4 indices from the observations and one-month lead time persistent and MME simulations. Compared with the persistent forecast, the results of the dynamical model slightly deviate from the observed Niño3.4 index. In general, the Niño3.4 index can be predicted well by both forecasts for a one-month lead time (with a TCC skill of 0.96). There is no additional gain from dynamical ENSO prediction for the forecast of the following month.

The skill of the persistent and MME forecasts at a one-month lead time (shown in Figure 1) increases as the forecast lead time increases (see Figure 11a). The TCC skill of the persistent forecast drastically decreases from one- to six-month lead times. On the other hand, the MME skill decreases very slowly and remains better than the individual model skills. This is due to the fact that the MME improves the skill related to the signal by resolving systematic errors and reducing random noise (see Introduction). The individual models have their own initialization strategies and consequently different systematic biases. In a similar way, Zhu et al. (2012) pointed out the importance of the multiple ocean analysis ensemble (MAE) initialization for the ENSO prediction. In addition to the initialization, a model dependency exists. For example, Meteorological Service of Canada (MSC) CGCM3 and CGCM4 have same ocean model and initialization strategies, except for the atmospheric model. They show different ENSO prediction skills due to air-sea coupling (indicated by light blue and purple markers, respectively).

The average skill of the individual models also decreases with the lead time and is better than the persistent forecast. With increasing lead time, the predictive skill decreases and the model spread increases. At the 6-month lead time, the skill of the individual models is the worst (~0.6; indicated by the dotted line in Figure 11). The June-November and December-May forecasts show similar decreasing trends, which are somewhat linear (Figures 11b and 11c), compared with all months combined (Figure 11a). It is relatively difficult to predict the Niño3.4 index during boreal summer than in winter (Sohn et al. 2016). This might be due to the seasonal phase locking of the ENSO prediction skills, which are relatively low in boreal summer at short-lead times (Barnston et al. 2012). The prediction skill of the dynamical models of the APCC one-tier six-month MME forecasts exceed that of the persistent forecast, in particular at long lead times with a big difference, and are predictable for approximately six months in advance, which is consistent with previous studies (Jin et al. 2008; Wang et al. 2009; Barnston et al. 2012; Imada et al. 2015). Various ENSO theories (Neelin et al. 1998; Wang 2001) support the fact that the prediction skill of ENSO is due to long oceanic memory-covering seasons.

On the other hand, the prediction errors of Niño3.4 forecasts increase and their model spread decreases when the lead times increase (see Figure 12). It seems that the increases of the error have little dependence on the predictive skill in terms of model consensus. A big model spread of the prediction errors was observed at the one-month lead; nonetheless, the models show better performance. Such error increases are not associated with the thermocline variability (Imada et al. 2015), which governs the prediction skill of ENSO.

To investigate the fluctuations of the Niño3.4 index of the individual model in detail, the time series of the monthly mean Niño3.4 index is shown in Figure 13. The models generally predict the ENSO variations with a considerable skill at short lead times and with decreasing skill levels at increasing lead times. This is due to the fact that most of the models are likely to predict the continuatiodn of the SST anomalies beyond the observation periods. The prediction skill of the persistent forecast is the worst because the same anomalous condition of the initial stage is maintained throughout the whole forecast period.

To summarize the ability to predict ENSO with lead times for the targeted forecast month, Figure 14 shows the TCC skills of the prediction of the Niño3.4 indices for each model. The persistent forecast shows a clear seasonal dependency of the prediction skill, which is mainly due to the phase locking of the ENSO to the annual cycle (Torrence and Webster 1998). This is the so-called “spring prediction barrier” (McPhaden 2003; Duan and Wei 2013); the evolution of the ENSO is more difficult to predict during boreal spring. The "spring prediction barrier" affects the dynamical models less than the persistent forecast. The correlation skill patterns of the models (Figure 14) are roughly comparable. At short lead times, the prediction skills show a relative minimum in summer.

## 4.2 Prediction skills of the tropical Pacific sea surface temperature and precipitation

Figure 15 shows how the ENSO strength affects the tropical Pacific SST and precipitation prediction skills based on MME. The SST and precipitation forecast skills are significantly correlated with the ENSO strength (with correlation coefficients of 0.64 and 0.57, respectively) from 1983 to 2005. The ENSO is the major signal factor in determining the prediction skill of the SST change and precipitation variability in the tropical Pacific region.

To examine the prediction skill of the tropical Pacific SST for each lead time, the ACC skills of the SST were computed (Figure 16). At the one-month lead time, the persistent forecast skill is slightly better than that of MME. Similar to the ENSO skill, the prediction skill of the persistent forecast gradually decreases as the lead time increases and reaches ~0.2 at the six-month lead time. The general MME skill is generally superior to any individual model skill in terms of the time-averaged ACC for all lead times and slowly decreases as the lead time increases. The MME skills are strongly associated with the ENSO strength throughout the whole forecast lead time. They are always better than the average skill of the individual models; the model spread at any lead time is fairly consistent. The seasonal dependency between summer and winter is not shown. Among the individual models, the Predictive Ocean-Atmosphere Model for Australia (POAMA) shows a slightly better skill than others. This is probably due to the fact that POAMA can provide forecasts of El Niño and Nina many months in advance (Cottrill et al. 2013).

With respect to the prediction skill of the tropical Pacific precipitation, the skills are relatively lower than those of SST (Figure 17). The persistent forecast skill is quite similar to the average skill of the individual models. Nonetheless, POAMA always has a better skill than other models. Because the model can simulate the spatial and temporal variability of the rainfall associated with the displacements of the Southern Pacific Convergence Zone (SPCZ) and ITCZ during La Nina and El Niño, it can also provide good rainfall predictions for the tropical Pacific regions (Cottrill et al. 2013). The MME skill is highly related to the ENSO strength during boreal winter. This indicates that the prediction skill of the tropical oceanic and atmospheric processes underlying ENSO highly depends on the prediction ability of ENSO of the coupled models.

## 4.3 Forecast skills and potential predictability of El Niño-Southern Oscillation diversity

### 4.3.1 Forecast skills of El Niño-Southern Oscillation diversities

The prediction skills of the ENSO diversities of the extended seasonal prediction systems up to six-month lead times of the APCC MME and its member models have been assessed. Figure 18 shows the prediction skills of the SST variability associated with the ENSO diversities. The ability to predict the ENSO diversities is limited and has a shorter lead time. The TCC prediction skill of the tropical Pacific SST is ~ 0.4 at the six-month lead time. However, the TCC skill of the SST variability related to the ENSO diversities is ~ 0.4 at the three-month lead time. The MME forecast skill is still much better than that of any other individual model. This indicates that the ENSO diversities can be predicted as signal by cancelling errors. To further investigate the seasonality of the prediction skill, the other targeted months were also investigated (Figure 19). The ACC skills of the persistent run sharply decease between 0.3 and 0.4 at the three-month lead time for the whole targeted period. The dynamical models have a slightly better skill than the persistent runs (except for APCC and Pusan National University; PNU). In general, the prediction skills, in particular the “spring prediction barrier”, have no seasonality.

Figure 20 shows the prediction skills of the tropical Pacific precipitation related to the ENSO diversities. Similar to SST, the skill of the ENSO diversities at a three-month lead time is almost the same as that of the precipitation prediction at a six-month lead time (ACC value of ~ 0.2).

The TCC skills of the observed and MME-predicted monthly mean SST anomalies were also computed. Figure 21 shows the results for the original and diversity-related SST variability based on all months. In general, the model predictions of the original SST variability perform well over the whole tropical Pacific Ocean; the maximum skill is indicated for the central to eastern equatorial Pacific region at a one-month lead time. At the three-month lead time, the MME maintains the same spatial TCC skill pattern but shows a decrease in value. At the six-month lead time, the skill decreases at the edges of the tropical Pacific, with a maximum skill close to the date line. The prediction skill of the SST variability related to the ENSO diversity is relatively lower than that of the original one. Maximum skills are determined close to the date line and in the far eastern Pacific. This difference indicates the ENSO-related signal, which is found over the eastern Pacific at a one-month lead time. However, the significant signal is observed in the western Pacific. In case of the precipitation, the significant skill was mainly detected in the equatorial tropical Pacific (Figure 22). The ENSO-related signal is found over the western Pacific.

### 4.3.2 Variance of the El Niño-Southern Oscillation diversities

Figure 23 and 24 show the variance of the SST and precipitation. A large variance in the ENSO-related SST characterizes old tongue regions. The MME captures the fluctuation well. The large variability of ENSO diversities is shown in the equatorial Pacific and border region of the tropics. The one-month lead time MME can capture the variability; however, the amplitude is smaller than that of the observations. The variability of the three-month lead time becomes much smaller.

The ENSO-related precipitation was determined in the central Pacific (around the date line). The one-month lead time MME captures the variability and center of action. The diversity-related precipitation was observed over the western Pacific. The MME captures the zonal position well, at one- and three-month lead times. However, the spatial pattern is quite different and the variance is very small.

The local maximum of the variance was calculated to summarize the results for the variance (Figure 25). The SST variance explained by ENSO is quite large and slightly decreases as the lead time increases. The model can capture the trend despite of the gap between them. The observations regarding the SST variability related to the ENSO diversities show very stable changes; however, but the MME suddenly decreases at a two-month lead time. In case of the precipitation, both the variability related to ENSO and that associated with the diversities are quite stable. However, the diversity-related variability is much larger than the ENSO variability. The model shows a decreasing trend in both cases; the diversity-related precipitation of the MME has relatively small amplitudes.

### 4.3.3 Potential predictability of El Niño-Southern Oscillation diversities

The predictability of the ENSO diversities using the dynamical seasonal climate prediction systems of several AOGCMs participating in the operational monthly six-month MME prediction at the APCC was accessed based on the PP (see Section 2). The results based on the one-month lead ensemble hindcasts of the individual models are plotted in Figure 26. The potentially predictable component of the regular ENSO signal-removed interannual variability is measured because the ENSO diversities are separated from the canonical ones. The models largely differ. The wide horse-shaped areas over the tropical Pacific represent the predictable part.

The area-averaging analyses of the PP of the ENSO diversities for each lead time reveal that the PP of the ENSO diversities is consistent with the prediction skill of the tropical SST variability (Figure 27a). However, note that the order of the individual models is different from that of the SST prediction skill (Figure 27b).

## 5. SUMMARY AND DISCUSSION

We diagnosed the ENSO and its response in terms of ENSO strengths/type, associated SST changes, and diversity in eight CGMCS included in the APCC MME seasonal prediction system. First of all, the skill of the APCC MME seasonal forecast system in predicting ENSO occurrences and the global SST was assessed based on retrospective forecasts targeting all seasons for the 1982–2006 period. In general, the seasonal SST predictability depends strongly on the ENSO phase and intensity. The models perform better in capturing the variations of the Niño3.4 index during strong ENSO events than during weak ENSO years. The global SST prediction skill is more sensitive to ENSO strength. Most strong El Niño events identified in the hindcast period belong to the canonical type of El Niño, whereas all weak El Niño events correspond to El Niño Modoki. During those strong events, the global SST changes were predicted well by the models. On the other hand, a number of models fail to reproduce the SST anomalies typically associated with El Niño Modoki (especially those over the far eastern Pacific), resulting in relatively poor MME skills in capturing global SST variations during weak El Niño years. During weak La Niña events, the models provide central to eastern Pacific SST signals, which are less persistent than the observations. The global SST forecasts also perform poorly compared with those during strong La Niña events.

Second, the accuracy of the coupled models predicting the ENSO diversity was assessed. The ENSO diversity is defined by the residual mode based on the difference between the total variability and forced mode of the canonical ENSO variability. Prior to the analysis of the prediction skill and predictability of the diversity, the conventional ENSO prediction has been compared with the observations. Both one-month lead time persistent and MME forecasts are skillful and capture the SST variability in the Niño3.4 region. However, as the lead time increases, the prediction skill of the persistent run decreases sharply; the skills of the MME and individual models are maintained even at a six-month lead time. The prediction skill of the boreal winter is much better that of the summer, which might be related to the spring barrier problem; the short lead time prediction skills have a relative minimum in summer. The correlation skills of the models are roughly comparable. The general MME skill is generally superior to the individual models. The Niño3.4

index, tropical Pacific SST, and precipitation prediction skill were compared with the diversity-related SST and precipitation prediction. The prediction skill of the tropical Pacific SST is ~0.4 at a six-month lead time; however, the prediction skill of the diversity-related SST has almost the same value at a three-month lead time. In case of the precipitation, the prediction skills of the variability at a six-month lead time and that of the diversity-related variability at a three-month lead time are equal (0.2). The ability to predict the ENSO diversity is limited and has a shorter lead time. In addition, the variance of the ENSO diversity is relatively smaller than the ENSO-related variability. With a small amplitude, the diversity is more affected by atmospheric noise and consequently prevents the development of an oceanic signal that can be used for the prediction (Imada et al. 2015). In addition to the prediction skill, the PP of the ENSO diversity was investigated to reveal the signal factor of the different types. The predictability source was determined over the whole tropical Pacific basin, except for NCEP. The exception of NCEP is probably related to the fact that NCEP is often likely to overestimate the ENSO and the large fractional variance of the canonical mode might be eliminated from the diversity of the NCEP model. Nonetheless, the PPs of the individual models appear to be stable at long lead times.

Because of the above-mentioned sensitivity of the SST prediction skills to the type of ENSO, more studies are needed to elucidate various mechanisms that trigger and sustain the ENSO and its diversity and how well these mechanisms are reproduced in state-of-the-art coupled models. It has been suggested that an irregular ENSO might be more affected by local air–sea coupling rather than basin-wide ocean dynamics (Kao and Yu 2009); how well these regional climate signals can be assimilated by Tier-1 climate prediction systems needs to be addressed. The reason for the difference between the PP and actual prediction skill should be further investigated.

Our results highlight the problem with respect to adopting a single index for ENSO predictions. Although it is the most widely used ENSO index, especially within the seasonal climate prediction community, the use of the Niño3.4 index alone might lead to the mixing of the two ENSO types. The Niño3.4 index alone, which is based on the SST over the central equatorial Pacific without taking conditions farther east into account, cannot distinguish between canonical and atypical El Niño events.

The two El Niño types are also known to show different teleconnection patterns and therefore very different climate impacts across the globe (Lakin and Harrison 2005). It is therefore imperative to differentiate between the signals related to different ENSO types to obtain more accurate information that can be used in regional climate assessments and seasonal forecasts. In addition, it is important to know the upper limits of the predictability and actual prediction skill of the ENSO diversity, which benefits the model improvement and better understanding of the ENSO prediction. The ENSO prediction is the core of seasonal climate forecasting. These results shed light on the challenging problem with respect to changes of the ENSO and diversity-related predictability.

## Acknowledgements

The authors thank the institutes participating in the APCC multi-model ensemble prediction for providing the 1-Tier hindcast experiment data. This research was supported by the APEC Climate Center.

## REFERENCE


Ajaya Mohan, R. S., and B. N. Goswami, 2003: Potential predictability of the Asian Summer monsoon on monthly and seasonal time scales. Meteorol. Atmos. Phys., 84, 83-100.

Alessandri, A., A. Borreli, S. Masina, A. Cherchi, S. Gualdi, A. Navarra, P. Di Pietro, and A Carril, 2010: The INGV-CMCC Seasonal Prediction System: improved ocean initial conditions. Mon. Wea. Rev., 138, 2930-2952.

An, S.-I., and F.-F. Jin, 2004: Nonlinearity and asymmetry of ENSO. J. Clim., 17, 2399-2412.

An, S.-I., and B. Wang, 2005: The forced and intrinsic low-frequency modes in the North Pacific. J. Clim., 18, 876-885.

Ashok, K., and T. Yamagata, 2009: The El Nino with a difference. Nature, 461, 481-484.

Ashok, K., S. K. Behera, S. A. Rao, H. Weng, and T. Yamagata, 2007: El Niño Modoki and its possible teleconnection. J. Geophys. Res., 112, C11007.

Barnston, A. G., 1994: Linear statistical short-term climate predictive skill in the Northern Hemisphere. J. Clim., 7, 1513-1564.

Barnston, A. G., M. K. Tippett, M. L. L'Heureux, S. Li, and D. G. DeWitt, 2012: Skill of real-time seasonal ENSO model predictions during 2002-11. Bull. Amer. Meteor. Soc., 93, 631-651.

Behera, S. K., J.-J. Luo, S. Masson, P. Delecluse, S. Gualdi, A. Navarra, and T. Yamagata, 2005: Paramount impact of the Indian Ocean dipole on the East African short rains: A CGCM study. J. Clim., 18, 4514-4530.

Behringer. M. J., and A. Leetmaa, 1998: An improved coupled model for ENSO prediction and implications for ocean initialization. Part I: The ocean data assimilation system. Mon. Wea. Rev., 126, 1013-1021.

Bellucci, A., S. Masian, P. Di Pietro, and A. Navarra, 2007: Using temperature-salinity relations in a global ocean implementation of a multivariate data assimilation scheme. Mon. Wea. Rev., 135, 3785-3807.

Boer, G. J., 2011: Decadal potential predictability of twenty-first century climate. Clim. Dyn., 36, 1119-1133.

Cai, W., and T. Cowan, 2009: La Niña Modoki impacts Australia autumn rainfall variability. Geophys. Res. Lett., 36, L12805.

Chen, G., and C.-Y. Tam, 2010: Different impacts of two kinds of Pacific Ocean warming on tropical cyclone frequency over the western North Pacific. Geophys. Res. Lett., 37, L01803.

Chen, W., H.-F. Graf, and R.-H. Huang, 2000: The interannual variability of East Asian winter monsoon and its relation to the summer monsoon. Adv. Atmos. Sci. 17, 48-60.

Coelho, C. A. S., S, Pezzulli, M. Balmaseda, F. J. Doblas-Reyes, and D. B. Stephenson, 2004: Forecast calibration and combination: A simple Bayesian approach for ENSO. J. Clim., 17, 1504-1516.

Colman, A. W., and M. K. Davey, 2003: Statistical prediction of global seas-surface temperature anomalies. Int. J. Climatol., 23, 1677-1697.

Cottrill, A., and coauthors, 2013: Seasonal forecasting in the Pacific using the coupled model POAMA-2. Weather Forecasting, 28, 668-680.

Covey, C., and coauthors, 2003: An overview of results from the Coupled Model Intercomparison Project (CMIP). Glob. Planet. Change, 37, 103-133.

DelSole, T., A. Kuma, and B. Jha, 2013: Potential seasonal predictability: Comparison between empirical and dynamical model estimates. Geophys. Res. Lett., 40, 3200-3206.

Doblas-Reyes, F. J., R. Hagedorn, and T. N. Palmer, 2005: The rationale behind the success of multi-model ensembles in seasonal forecasting - II. Calibration and combination. Tellus, 57A, 234-252.

Duan, W., and C. Wei, 2013: The 'spring predictability barrier' for ENSO predictions and its possible mechanism: results from a fully coupled model. Int. J. Climatol., 33, 1280-1292.

Feng, J., W. Chen, C.-Y. Tam, and W. Zhou, 2011: Different impacts of El Niño and El Niño Modoki on China rainfall in the decaying phases. Int. J. Climatol., 31, 2091-2101.

Feng, J., J. Li, F. Zheng, F. Xie F, and C. Sun, 2016: Contrasting impact of developing phases of two types of El Niño on southern China rainfall. J. Meteor. Soc. Jpn. 94, 359-370.

Goddard, L., and N. E. Graham, 1999: Importance of the Indian Ocean for simulating rainfall anomalies over eastern and southern Africa. J. Geophys. Res., 104, 19099-19116.

Goddard, L., S. J. Mason, S. E. Zebiak, C. F. Ropelewski, R. Basher, and M. A.Cane, 2001: Current approaches to seasonal to interannual climate predictions. Int. J. Climatol., 21, 1111-1152.

Guilyardi, E., A. Wittenberg, A. Fedorov, M. Collins, C. Wang, A. Capotondi, G. J. von Oldenborgh, T. Stockdale, 2009: Understanding El Nino in ocean-atmosphere general circulation models: Progress and challenges. Bull. Amer. Meteor. Soc. 90, 325-340.

Ham, Y. G., S. Schubert, and Y. Chang, 2012: Optimal initial perturbations for ensemble prediction of the Madden-Julian oscillation during boreal winter. J. Clim., 25, 4932-4945.

Ham, Y. G., S. Schubert, Y. Vikhliaev, and M. J. Suarez, 2014: An assessment of the ENSO forecast skill of GEOS-5 system. Clim. Dyn., 43, 2415-2430.

Hudson, D., O. Alves, H. H. Hendon, G. Wang, 2010: The impact of atmospheric initialization on seasonal prediction of tropical Pacific SST. Clim. Dyn., 36, 1155-1171.

Imada, Y., H. Tatebe, M. Ishi, Y. Chikamoto, M. Mori, M. Arai, M. Watanabe, M. Kimoto, 2015: Predictability of two types of El Nino assessed using an extended seasonal prediction system by MIROC. J. Clim., 143, 4597-4617.

Infanti, J. M., and B. P. Kirtman, 2016: North American rainfall and temperature prediction response to the diversity of ENSO. Clim. Dyn., 46, 3007-3023.

Janowiak, J. E., and P. Xie, 1999: CAMS_OPI: A global satellite-rain gauge merged product for real-time precipitation monitoring applications. J. Clim., 12, 3335-3342.

Jeong, H. I., and coauthors, 2008: Experimental 6-month hindcast and forecast simulations using CCSM3, APCC 2008 Technical Report, APEC Climate Center

Jin, E. K., J. L. Kinter III, B. Wang, C. K. Park, I. S. Kang, B. P. Kirtman, J. S. Kug, A. Kumar, J. J. Luo, J. Schemm, J. Shukla, and T. Yamagata, 2008: Current status of ENSO prediction skill in coupled ocean-atmosphere models. Clim. Dyn., 31, 647-664.

Kao, H.-Y., and J.-U. Yu, 2009: Contrasting eastern-Pacific and central-Pacific types of ENSO. J. Clim., 22, 615-632.

Kaori, M. A., J. Li, and F. F. Jin, 2013: The asymmetric influence of the two types of El Nino and La Nina on summer rainfall over southeast China. J. Clim., 26, 4567-4582.

Kim, H. J., and J. B. Ahn, 2015: Improvement in prediction of the Arctic Oscillation with a realistic ocean initial condition in a CGCM. J. Clim., 28, 8951-8967.

Kosaka, Y., and H. Nakamura, 2006: Structure and dynamics of the summertime Pacific-Japan teleconnection pattern. Q. J. R. Meteorol. Soc., 132, 2009-2030.

Krishnan, R., C. Zhang, and M. Sugi, 2000: Dynamics of breaks in the Indian summer monsoon. J. Atmos. Sci., 57, 1354-1372.

Kug, J.-S., J.-Y. Lee, and I.-S. Kang, 2007: Global sea surface temperature prediction using a multimodel ensemble, Mon. Wea. Rev., 135, 3239-3247.

Kug, J.-S., F.-F. Jin, and S. I. An, 2009: Two types of El Niño events: cold tongue El Niño and warm pool El Niño. J. Clim., 22, 1499-1515.

Kug, J. S., M. S. Ahn, M. K. Sung, S. W. Yeh, H. S. Min, and Y. H. Kim, 2010: Statistical relationship between two types of El Niño events and climatic variation over the Korean Peninsula. Asia. Pac. J. Atmos. Sci., 46, 467-474.

Kug, J.-S., and Y.-G. Ham, 2011: Are there two types of La Niña? Geophys. Res. Lett., 38, L16704.

Larkin, N.-K., and D. E. Harrison, 2005: Global seasonal temperature and precipitation anomalies during El Niño autumn and winter. Geophys. Res. Lett., 32, L16705.

Lau, N.-C., 1997: Interaction between global SST anomalies and the midlatitudes atmospheric circulation. Bull. Amer. Meteor. Soc., 78, 21-33.

Lau, N.-C., and B. Wang, 2005: Monsoon-ENSO interaction, in The Global Monsoon System: Research and Forecast, edited by C.-P. Chang, B. Wang, and N.-C. G. Lau, WMO/TD No. 1266.

Li, G, and S. P Xie, 2014: Tropical biases in CMIP5 multimodel ensemble: The excessive equatorial Pacific cold tongue and double ITCZ problems. J. Clim., 27, 1765-1780.

Luo, J. J., S. Masson, E. Roeckner, G. Madec, and T. Yamagata, 2005: Reducing climatology bias in an ocean-atmosphere CGCM with improved coupling physics. J. Clim., 18, 2344-2360.

McPhaden, M. J., 2003: Tropical Pacific Ocean heat content variations and ENSO persistence barriers. Geophys. Res. Lett., 30, 1480.

Meehl, G. A., and J. M. Arblaster, 2002: Indian monsoon GCM sensitivity experiments testing tropospheric biennial oscillation transition conditions. J. Clim., 15, 923-944.

Merryfield, W. J., W. S. Lee, G. J. Boer, V. V. Kharin, J. F. Scinocca, G. M. Flato, R. S. Ajayamoham, J. C. Fyfe, Y. Tang, and S. Polavarapu, 2013: The Canadian seasonal to interannual prediction system. Part I: Models and initialization. Mon. Wea. Rev., 141, 2910-2945.

Misra, V., L. Marx, M. Brunke, and X. Zeng, 2008: The equatorial Pacific cold tongue bias in a coupled climate model. J. Clim., 21, 5852–5869.

Neelin, J., D. Battisti, A. Hirst, F.-F. Jin, T. W. T. Yamagata, and S. Zebiak, 1998: ENSO theory. J. Geophys. Res., 103, 14261–14290.

Nitta, T., 1987: Convective activities in the tropical Pacific and their impacts on the Northern Hemisphere summer circulation. J. Meteorol. Soc. Jpn., 65, 373–390.

Phelps, M. W., A. Kumar, and J. J. O'Brien, 2004: Potential predictability in the NCEP CPC dynamical seasonal forecast system. J. Clim., 17, 3775–3785.

Rasmusson, E. M., and T. H. Carpenter, 1982: Variation in tropical sea surface temperature and surface wind fields associated with the Southern Oscillation/El Niño. Mon. Wea. Rev., 110, 354–384.

Rasmusson, E. M., and J. W. Wallace, 1983: Meteorological aspects for the El Niño/Southern Oscillation. Science, 222, 1195–1202.

Reynolds, R. W., N. A. Rayner, T. M. Smith, D. C. Stokes, and W. Wang, 2002: An improved tin situ and satellite SST analysis for climate. J. Clim., 15, 1609–1625.

Roads, J. O., S. C. Chen, and F. Fujioka, 2001: ECPC's weekly to seasonal global forecast. Bull. Amer. Meteor. Soc., 82, 639–658.

Rowell, D. P., 1998: Assessing potential seasonal predictability with an ensemble of multidecadal GCM simulations. J. Clim., 11, 109–120.

Ropelewski, C. F., and M. S. Halpert, 1987: Global and regional scale temperature patterns associated with the El Niño/Southern Oscillation. Mon. Wea. Rev., 115, 1606–1626.

Ropelewski, C. F., and M. S. Halpert, 1996: Quantifying Southern Oscillation-precipitation relationships. J. Clim., 9, 1043–1059.

Saha, S., and coauthors, 2014: The NCEP climate forecast system version 2. J. Clim., 27, 2185–2208.

Sahai, A. K., A. M. Grimm, V. Satyan, and G. B. Pant, 2003: Long-lead prediction of Indian summer monsoon rainfall from global SST evolution. Clim. Dyn., 20, 855–863.

Shukla, J., L. Marx, D. Paolino, D. Straus, J. Anderson, J. Ploshay, D. Baumhefner, J. Tribbia, C. Brankovic, T. Palmer, Y. Chang, S. Schubert, M. Suarez, and E. Kalnay, 2000: Dynamical Seasonal Prediction. Bull. Amer. Meteor. Soc., 81, 2593–2606.

Sohn, S.-J., C.-Y. Tam, and J. B. Ahn, 2013: Development of a multimodel-based seasonal prediction system for extreme droughts and floods: a case study for South Korea. Int.

J. Climatol. 33, 793-805.

Sohn, S.-J., C.-Y. Tam, H.-I. Jeong, 2016: How do the strength and type of ENSO affect SST predictability in coupled models. Sci. Rep., 6: 33790.

Sun, J. Q., and J. B. Ahn, 2011: A GCM-based forecasting model for the landfall of tropical cyclones in China. Adv. Atmos. Sci., 28, 1049-1055.

Torrence, C., and P. J. Webster, 1998: The annual cycle of persistent in the El Nino/Southern Oscillation. J. Roy. Meteor. Soc., 124, 1985-2004.

Trenberth, K. E., 1997: The definition of El Niño. Bull. Amer. Meteor. Soc., 78, 2771-2777.

Trenberth, K. E., and J. M. Caron, 2000: The Southern Oscillation revisited: Sea level pressures, surface temperature and precipitation. J. Clim., 13, 4358-4365.

Waliser, D. E., K. M. Lau, W. Stern, and C. Jones, 2003: Potential predictability of the Madden-Julian Oscillation. Bull. Amer. Meteor. Soc., 84, 33-50.

Wang, B., R. Wu, and X. Fu, 2000: Pacific-East Asian teleconnection: How does ENSO affect East Asian Climate? J. Clim., 13, 1517-1536.

Wang, B., and coauthors, 2009: Advance and prospectus of seasonal predictions: Assessment of the APCC/CliPAS 14-model ensemble retrospective seasonal prediction (1980-2004). Clim. Dyn., 33, 93-117.

Wang, C., 2001: A unified oscillator model for the El Nino-Southern Oscillation. J. Clim., 14, 98-115.

Wang, L., W. Chen, and R. Huang, 2008: Interdecadal modulation of PDO on the impact of ENSO on the East Asian winter monsoon. Geophys. Res. Lett., 35(20), L20702.

Weng, H., S. K. Behera, and T. Yamagata, 2009: Anomalous winter climate conditions in the Pacific rim during recent El Niño Modoki and El Niño events. Clim. Dyn., 32, 663-674.

Xu, K., C. Zhu, and J. He, 2013: Two types of El Niño-related Southern Oscillation and their different impacts on global land precipitation. Adv. Atmos. Sci., 30, 1743-1757.

Yin, Y., O. Alves, and P. R. Oke, 2011: An ensemble ocean data assimilation system for seasonal prediction. Mon. Wea. Rev.,139, 786-808.

Yoo, J. H., and I. S. Kang, 2005: Theoretical examination for a multi-model composite for seasonal prediction. Geophys. Res. Lett., 32, L18707.

Yu, J. Y., Y. Zou, S. T. Kim, and T. Lee, 2012: The changing impact of El Nino on US winter temperatures. Geophys. Res. Lett., 39, L15702.

Yuan, Y., and H. M. Yan, 2013: Different types of La Niña events and different responses of the tropical atmosphere. Chin. Sci. Cull., 58, 406-415.

Zhang, Y., K. R. Sperber, and I. S. Boyle, 1997: Climatology and interannual variation of East Asian winter monsoon: Results from the 1979-1995 NCEP/NCAR reanalysis. Mon. Wea. Rev., 125, 2605-2619.

Zhou, L. T., C.-Y. Tam, W. Zhou, and J. C. L. Chan, 2010: Influence of South China Sea SST and ENSO on winter rainfall over South China. Adv. Atmos. Sci., 27(4), 832-844.

Zhu, J., B. Huang, L. Marx, L. Kinter III, M. A. Balmaseda, R.-H. Zhang, and Z. Z. Hu, 2012: Ensemble ENSO hindcasts initialized from multiple ocean analyses. Geophys. Res. Lett., 39, L09602.

# TABLE

**Table 1** Acronyms of institutions and models used in the text.

| Acronym | Full names |
|---|---|
| APCC | Asia-Pacific Economic Cooperation Climate Center |
| BOM | Bureau of Meteorology |
| CCCma | Canadian Centre for Climate Modeling and Analysis |
| CCSM | Community Climate System Model |
| CFS | Climate Forecast System |
| CMCC | Centro Euro-Mediterraneo per i Cambiamenti Climatici |
| GMAO | Global Modeling and Assimilation Office |
| MSC | Meteorological Service of Canada |
| NASA | National Aeronautics and Space Administration |
| NCEP | National Center for Environmental Prediction |
| PNU | Pusan National University |
| POAMA | Predictive Ocean-Atmosphere Model for Australia |
| SPS | Seasonal Prediction System |

Table 2 Description of the eight coupled climate models used in this study.

| Country | Institute | Model | AGCM/resolution | OGCM/resolution | Ensemble Member | Period | Reference |
|---|---|---|---|---|---|---|---|
| Australia | BOM | POAMA2.4 | BAMv3.0d/T47L17 | ACOM2/0.5–1.5°lat×2°lon L25 | 33 | 1983–2011 | Cottrill et al. (2013) |
| Canada | MSC | CCCma CGCM3 | AGCM3/T63L31 | OGCM4 (1.41°lon×0.94°lat L40) | 10 | 1982–2010 | Merryfield et al. (2013) |
| | MSC | CCCma CGCM4 | AGCM4/T63L31 | | 10 | 1982–2010 | |
| Italy | CMCC | CMCC–SPSv2 | ECHAM5.3/T63L19 | OPA8.2/ORCA2 grid_L31 | 9 | 1982–2005 | Alessandri et al. (2010) |
| Korea | APCC | CCSM3 | CAM3/T85L26 | POP1.3/Gxlv3_L40 | 5 | 1983–2014 | Jeong et al. (2008) |
| | PNU | PNU | CCM3/T42L18 | MOM3/0.7–2.8 lat L29 | 5 | 1981–2012 | Sun and Ahn (2011) |
| USA | NASA | GMAO | GEOS–5/288x181L72 | MOM4/720×410 L40 | 11 | 1982–2011 | Ham et al. (2012, 2014) |
| | NCEP | CFSv2 | GFS/T126L64 | MOM4/⅓°lat×1°lon L40 | 17 | 1983–2005 | Saha et al. (2014) |

**Table 3** Brief description of the initialization strategies of the models in the study.

| Model | Atmospheric Initialization | Ocean Initialization |
|---|---|---|
| POAMA2.4 | Atmosphere and land initialization scheme (ALI) for realistic initial conditions by nudging (Hudson et al. 2010) | POAMA Ensemble Ocean Data Assimilation System (PEODAS) based on an ensemble Kalman filter (Yin et al. 2011) |
| CCCma CGCM 3 and 4 | Burst initial conditions by Incremental Analysis Update (IAU; no lagged initial conditions; Merryfield et al. 2013) | SST nudging and assimilation |
| CMCC-SPSv2 | Spectral and time interpolation (INTERA) | CMCC-INGV Global Ocean Data Assimilation System based on (CIGODAS; Bellucci et al. 2007) based on the reduced-order optimal interpolation scheme |
| APCC | Lagged initial conditions | 3-dimensional (3D) nudging |
| PNU | Lagged initial conditions | Variational method using a filter (VAF; Kim and Ahn 2015) |
| GMAO | Breeding and random perturbation (Ham et al. 2014) | Ensemble Optimal Interpolation (EnOI) analysis scheme |
| CFSv2 | Lagged initial conditions | Modified 3D variation data assimilation to include vertical variations in the error covariances (Behringer et al. 1998) |

**Table 4** Classification of the ENSO events.

| | JFM | FMA | MAM | AMJ | MJJ | JJA | JAS | ASO | SON | OND | NDJ | DJF | ENSO Type |
|---|---|---|---|---|---|---|---|---|---|---|---|---|---|
| 1982 | -0.05 | -0.01 | 0.26 | 0.68 | 0.9 | 1.03 | 1.1 | 1.46 | 1.82 | 2.26 | 2.57 | 2.65 | SE |
| 1983 | 2.33 | 1.75 | 1.28 | 0.89 | 0.5 | 0.08 | -0.23 | -0.49 | -0.77 | -1 | -1.03 | -0.81 | WL |
| 1984 | -0.64 | -0.46 | -0.5 | -0.63 | -0.66 | -0.68 | -0.53 | -0.64 | -0.89 | -1.33 | -1.45 | -1.41 | WL |
| 1985 | -1.24 | -1.16 | -1.02 | -0.94 | -0.8 | -0.67 | -0.57 | -0.57 | -0.62 | -0.61 | -0.68 | -0.78 | WL |
| 1986 | -0.84 | -0.66 | -0.5 | -0.28 | -0.13 | 0.09 | 0.28 | 0.53 | 0.81 | 1.02 | 1.19 | 1.25 | WE |
| 1987 | 1.25 | 1.16 | 1.03 | 1.07 | 1.27 | 1.58 | 1.7 | 1.64 | 1.53 | 1.32 | 1.12 | 0.8 | SE |
| 1988 | 0.43 | 0.02 | -0.58 | -1.13 | -1.57 | -1.7 | -1.67 | -1.84 | -2.12 | -2.45 | -2.45 | -2.12 | SL |
| 1989 | -1.82 | -1.45 | -1.19 | -0.96 | -0.76 | -0.68 | -0.62 | -0.61 | -0.57 | -0.46 | -0.31 | -0.09 | |
| 1990 | 0.03 | 0.15 | 0.16 | 0.08 | 0 | 0.01 | 0.03 | 0.12 | 0.08 | 0.2 | 0.26 | 0.29 | |
| 1991 | 0.16 | 0.09 | 0.21 | 0.46 | 0.63 | 0.68 | 0.55 | 0.62 | 0.82 | 1.31 | 1.62 | 1.84 | SE |
| 1992 | 1.72 | 1.57 | 1.35 | 0.98 | 0.65 | 0.2 | -0.05 | -0.31 | -0.31 | -0.17 | 0.02 | 0.16 | |
| 1993 | 0.24 | 0.48 | 0.74 | 0.8 | 0.64 | 0.33 | 0.19 | 0.14 | 0.22 | 0.21 | 0.17 | 0.02 | |
| 1994 | -0.06 | -0.02 | 0.12 | 0.22 | 0.22 | 0.31 | 0.28 | 0.5 | 0.75 | 1.1 | 1.18 | 1.02 | WE |
| 1995 | 0.69 | 0.41 | 0.13 | -0.02 | -0.14 | -0.28 | -0.55 | -0.86 | -1.05 | -1.14 | -1.07 | -1.03 | WL |
| 1996 | -0.91 | -0.75 | -0.59 | -0.5 | -0.41 | -0.33 | -0.35 | -0.44 | -0.51 | -0.57 | -0.62 | -0.6 | |
| 1997 | -0.52 | -0.2 | 0.21 | 0.72 | 1.21 | 1.66 | 1.99 | 2.29 | 2.52 | 2.68 | 2.7 | 2.5 | SE |
| 1998 | 2.05 | 1.46 | 0.95 | 0.19 | -0.46 | -1.09 | -1.21 | -1.3 | -1.37 | -1.62 | -1.73 | -1.71 | SL |
| 1999 | -1.47 | -1.21 | -1.05 | -1.08 | -1.08 | -1.22 | -1.23 | -1.31 | -1.41 | -1.63 | -1.91 | -1.92 | SL |
| 2000 | -1.76 | -1.34 | -1.04 | -0.85 | -0.77 | -0.65 | -0.63 | -0.72 | -0.86 | -1 | -1.01 | -0.93 | WL |
| 2001 | -0.75 | -0.54 | -0.4 | -0.25 | -0.15 | -0.05 | -0.12 | -0.18 | -0.26 | -0.33 | -0.31 | -0.19 | |
| 2002 | -0.05 | 0.05 | 0.11 | 0.36 | 0.58 | 0.8 | 0.91 | 1.11 | 1.34 | 1.49 | 1.46 | 1.18 | WE |
| 2003 | 0.82 | 0.43 | 0.01 | -0.24 | -0.2 | -0.02 | 0.11 | 0.21 | 0.34 | 0.38 | 0.3 | 0.2 | |
| 2004 | 0.02 | -0.03 | 0 | 0.1 | 0.22 | 0.39 | 0.6 | 0.69 | 0.71 | 0.72 | 0.69 | 0.54 | WE |
| 2005 | 0.36 | 0.27 | 0.3 | 0.32 | 0.31 | 0.22 | 0.03 | -0.05 | -0.19 | -0.4 | -0.72 | -0.84 | |

**Table 5** El Niño and La Niña events[3].

| El Niño | | La Niña | |
|---|---|---|---|
| Strong | Weak | Strong | Weak |
| 1982-1983 | 1986-1987* | 1988-1989** | 1983-1984** |
| 1987-1988 | 1994-1995* | 1998-1999** | 1984-1985 |
| 1991-1992* | 2002-2003* | 1999-2000 | 1985-1986 |
| 1997-1998 | 2004-2005* | | 1995-1996 |
| | | | 2000-2001** |
| 4 cases | 4 cases | 3 cases | 5 cases |

3) * and ** correspond to the El Niño Modoki and La Niña Modoki events, respectively. See text for details.

FIGURE

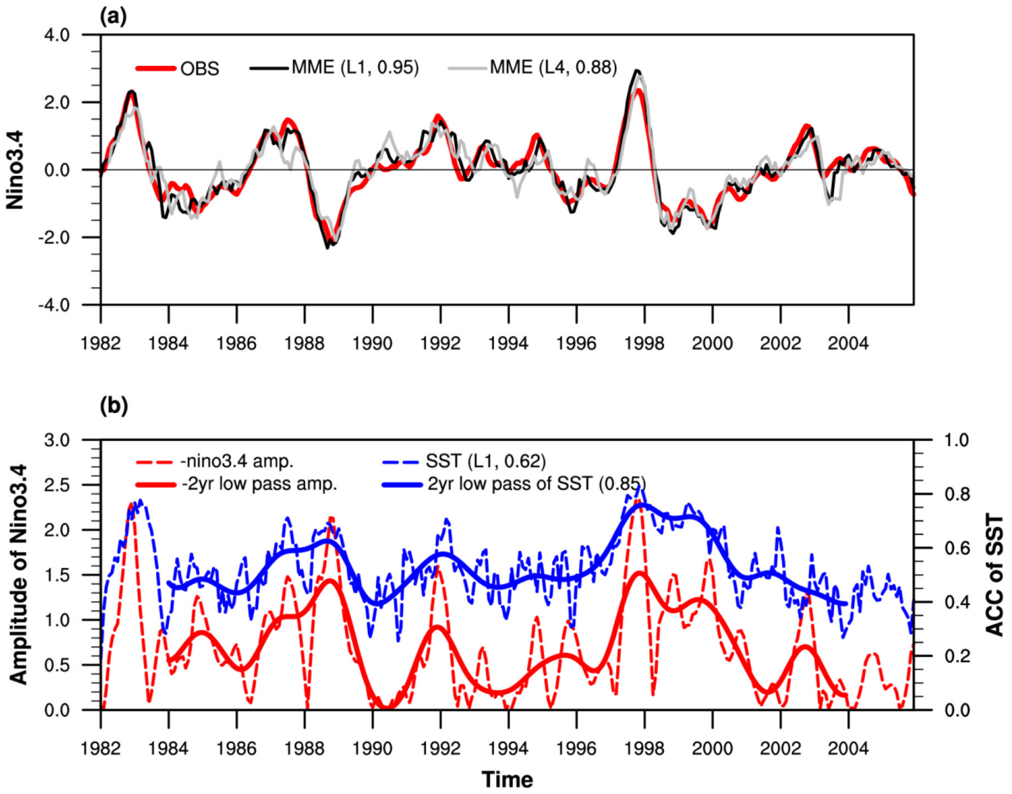


**Figure 1** (a) Time series of the monthly mean Niño3.4 index from observations (red line); one-month (black) and four-month (grey) lead time multi-model ensemble (MME) simulations with year-round three-month running average within the period from 1982 to 2006. The correlation coefficients between the observed and MME-simulated indices are given in parentheses following the legends. (b) Time series of the observed amplitude (absolute value of Figure 1a) of Niño3.4 (red dashed line) and anomaly pattern correlation (ACC) skill of the global sea surface temperature (SST) (60°S–80°N, 0°–330°E) prediction (blue dashed line). The solid lines show the two-year lowpass-filtered data of the former two time series.

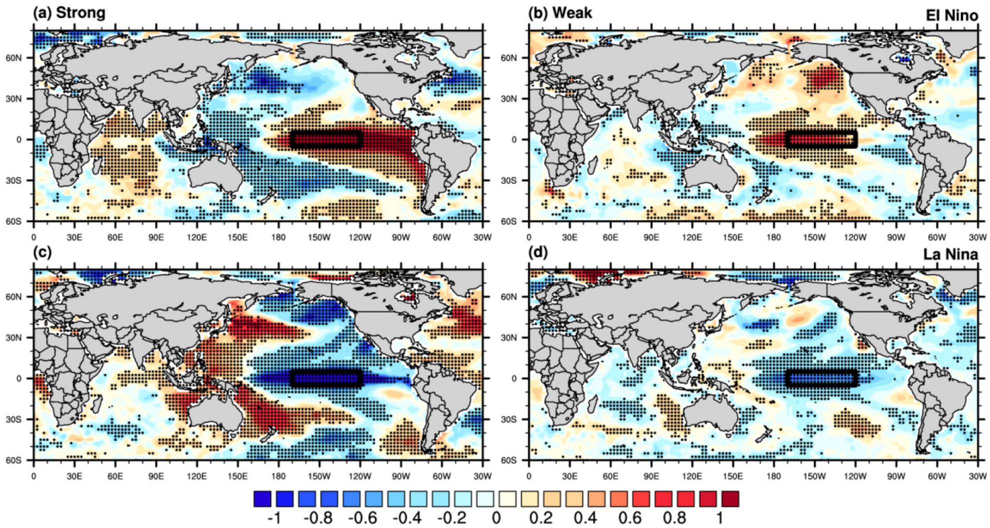


Figure 2 Composite maps of anomalous sea surface temperature (SST; shading) during (a, b) El Niño and (c, d) La Niña phases corresponding to (a, c) strong and (b, d) weak El Niño–Southern Oscillation (ENSO) events in the boreal warm season. The black dots indicate grid points, where anomalies are statistically significant at the 95% level. The Niño3.4 region is denoted by a rectangular box in each panel.

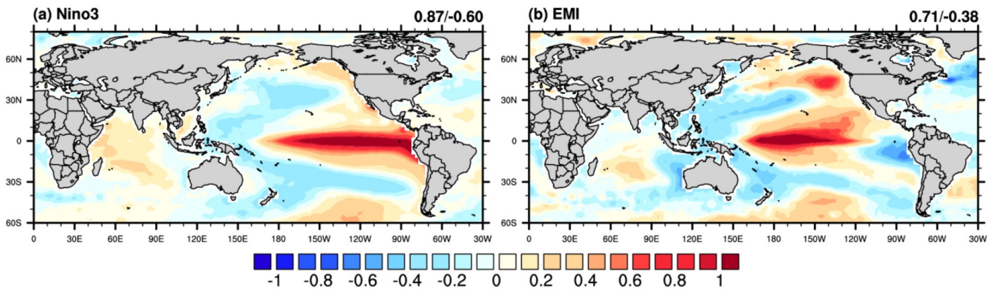


Figure 3 Regression coefficients of the sea surface temperature (SST) of the (a) Niño3 index and (b) El Niño Modoki index (EMI) based on the observations for all seasons during 1982–2006. The pattern correlation coefficients between the regression map based on the Niño 3 index (EMI) and strong El Niño/La Niña composites (weak El Niño/La Niña composites) during the boreal warm season are presented in the upper right corner of each panel.

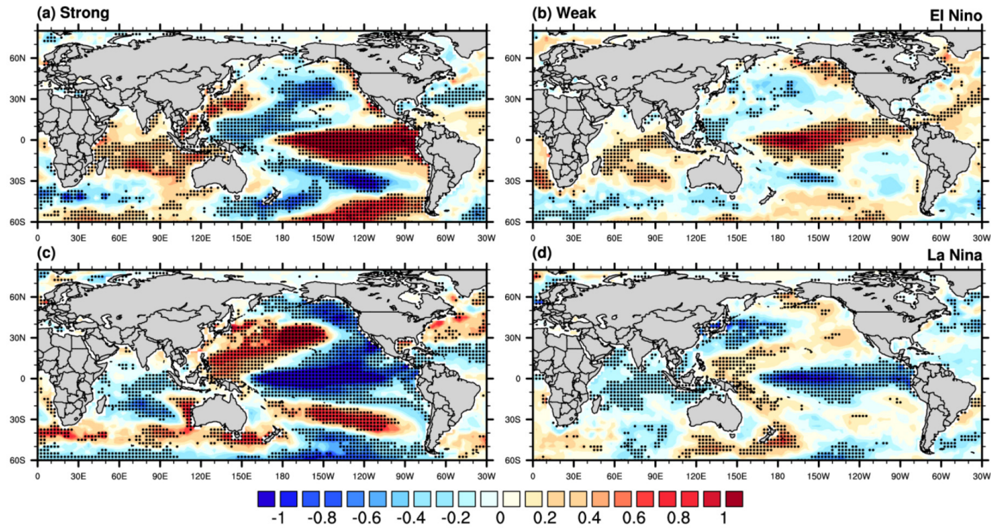


**Figure 4** Composite maps of the anomalous sea surface temperature (SST; shading) during (a, b) El Niño and (c, d) La Niña phases for (a, c) strong and (b, d) weak El Niño-Southern Oscillation (ENSO) events during the boreal cold season. The black dots indicate grid points; the anomalies are statistically significant at the 95% level.

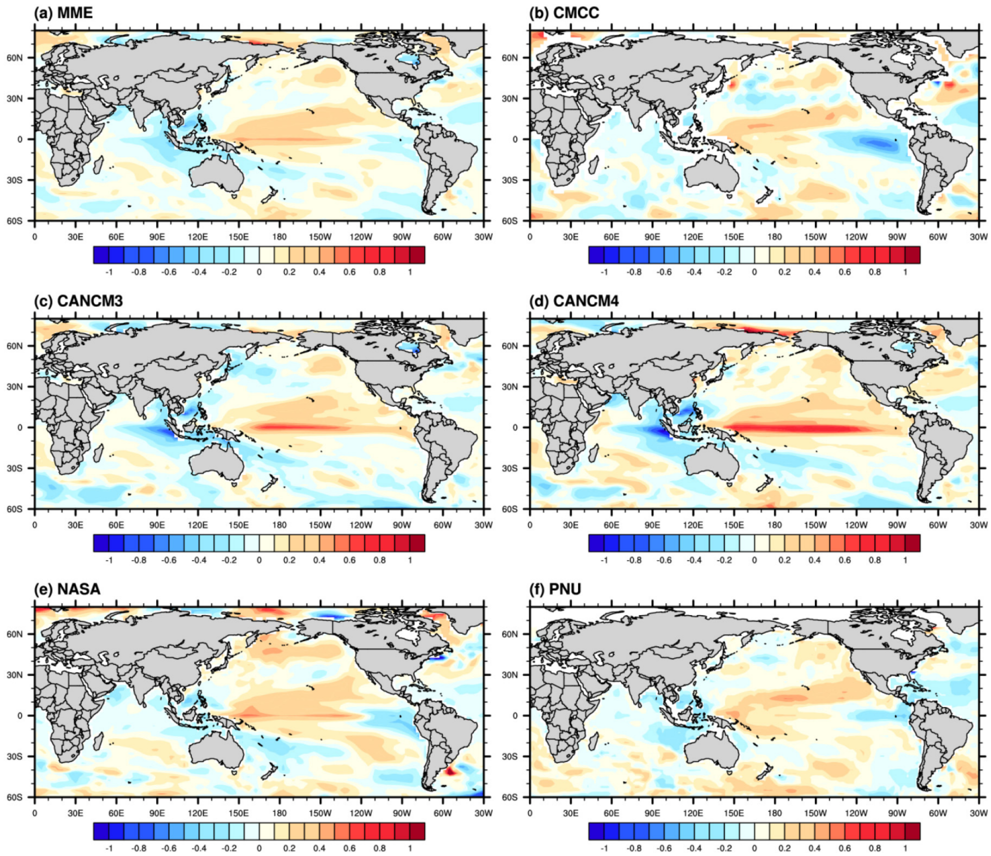


**Figure 5** Composite maps of anomalous sea surface temperature (SST; shading) for weak El Niño events during the boreal warm season based on (a) multi-model ensemble (MME) mean and individual model simulations from (b) CMCC, (c) MSC CGCM3, (d) MSC CGCM4, (e) NASA and (f) PNU.

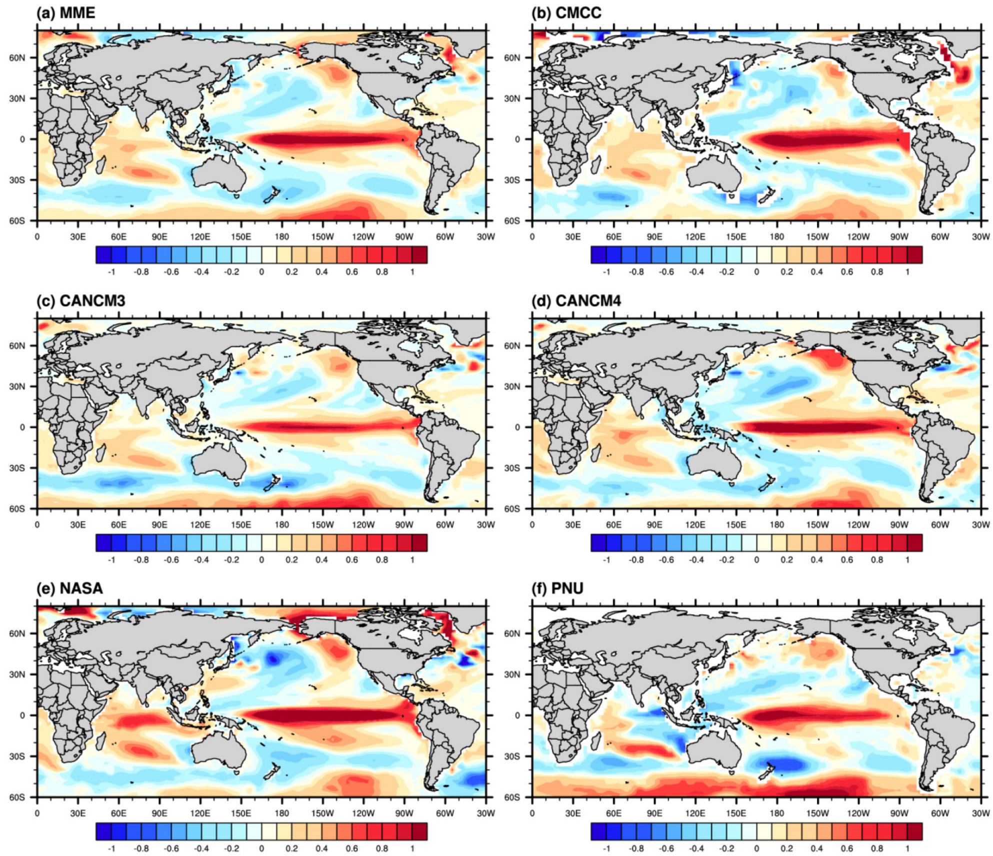


Figure 6 Composite maps of the anomalous sea surface temperature (SST; shading) during weak El Niño events in the boreal cold season based on (a) multi-model ensemble (MME) mean and simulations from (b) CMCC, (c) MSC CGCM3, (d)MSC CGCM4, (e) NASA and (f) PNU.

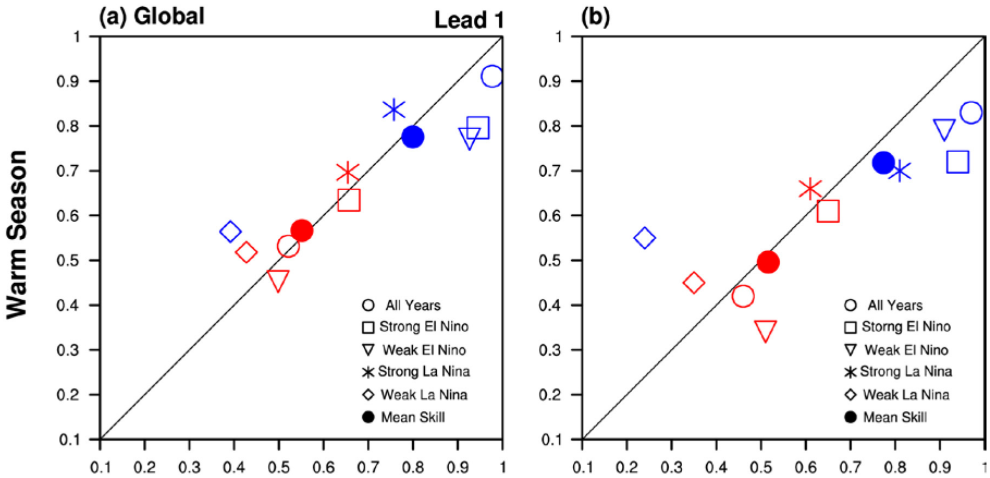


Figure 7 Skills of the Niño3.4 index forecasts (in blue) and sea surface temperature (SST) pattern forecasts across the globe (in red) during boreal cold (x-axis) and warm (y-axis) seasons for all years and strong El Niño, weak El Niño, strong La Niña, and weak La Niña events (see legends in figures), respectively, based on (a) one-month lead times and (b) August and November-initiated multi-model ensemble (MME) simulations. The index forecast skill is defined as the correlation between the observed and simulated MME mean Niño3.4 index based on the samples of case numbers of each event multiplied by the period of each season. The SST pattern forecast skill is defined as the anomaly pattern correlation between the SSTs from observations and MME simulations.

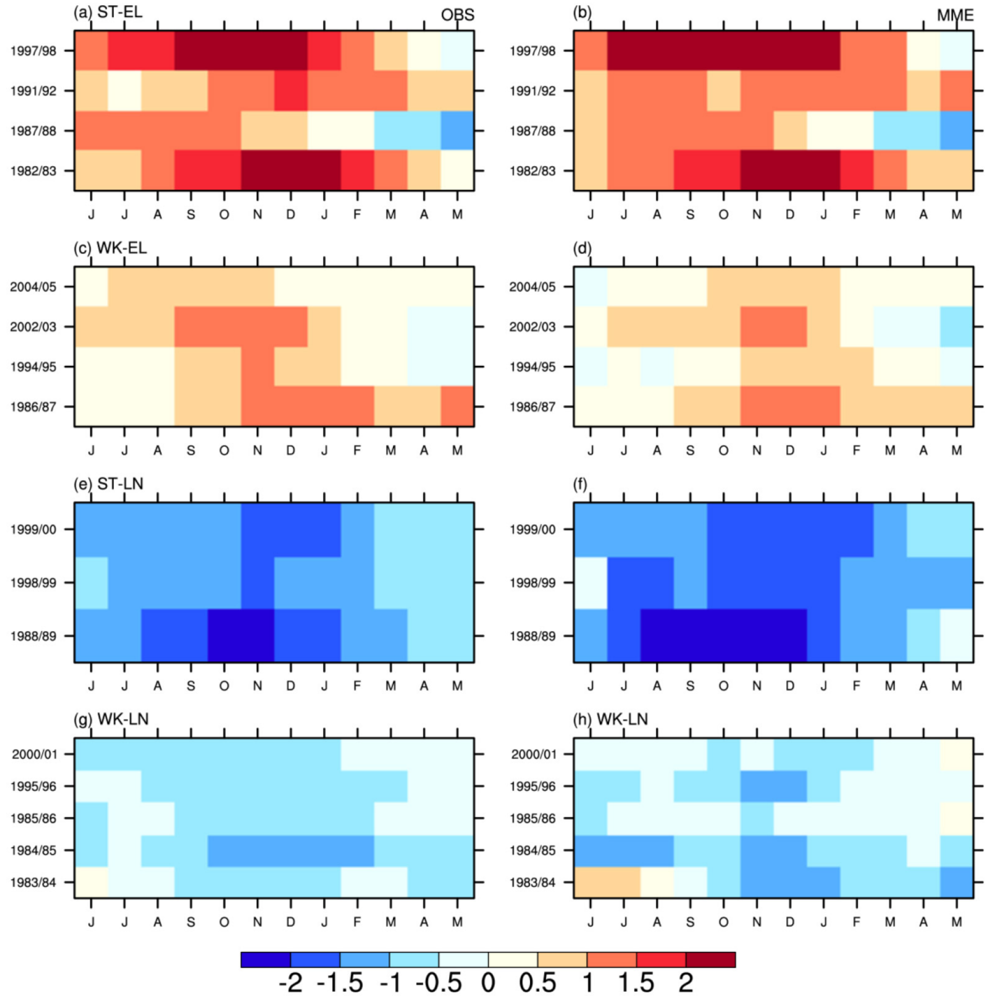


Figure 8 Evolution of the observed (left panels) and multi-model ensemble (MME) mean (right panels) forecasted Niño3.4 index for (a, b) strong El Niño, (c, d) weak El Niño, (e, f) strong La Niña, and (g, h) weak La Niña events.

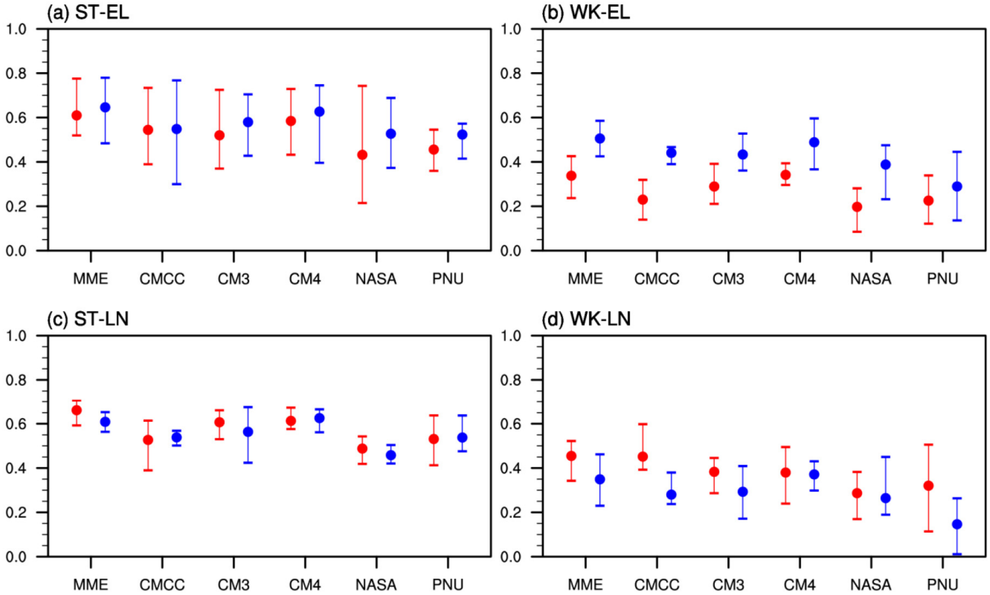


Figure 9 Mean (solid dot) and range (bar) of the anomaly pattern correlation coefficients (ACCs) between the observed and model-simulated sea surface temperature (SST) patterns based on data from (a) strong El Niño, (b) weak El Niño, (c) strong La Niña, and (d) weak La Niña years. The red and blue values denote the statistics for warm and cold seasons, respectively.

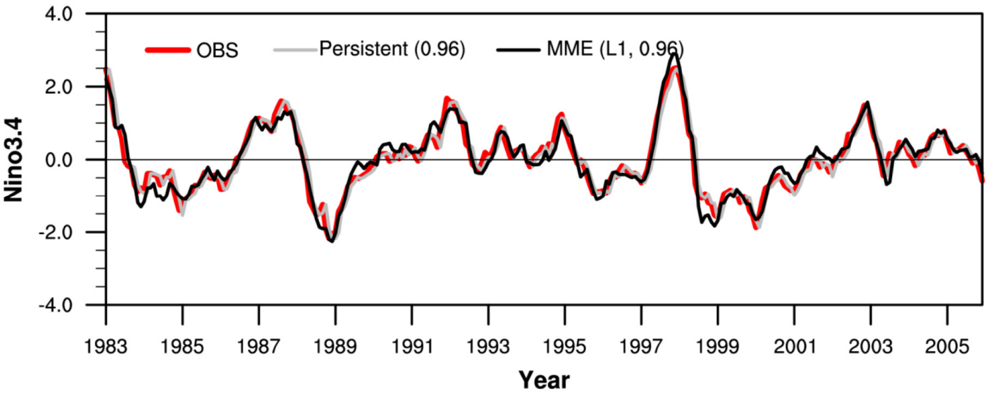


Figure 10 Time series of the monthly mean Niño3.4 index from observations (red line), persistent (grey), and one-month lead time multi-model ensemble (MME; black) simulations for the whole year within the period from 1983 to 2005. The temporal correlation coefficient (TCC) skill between the observed and persistent (MME-simulated) indices is given in parentheses following the legends.

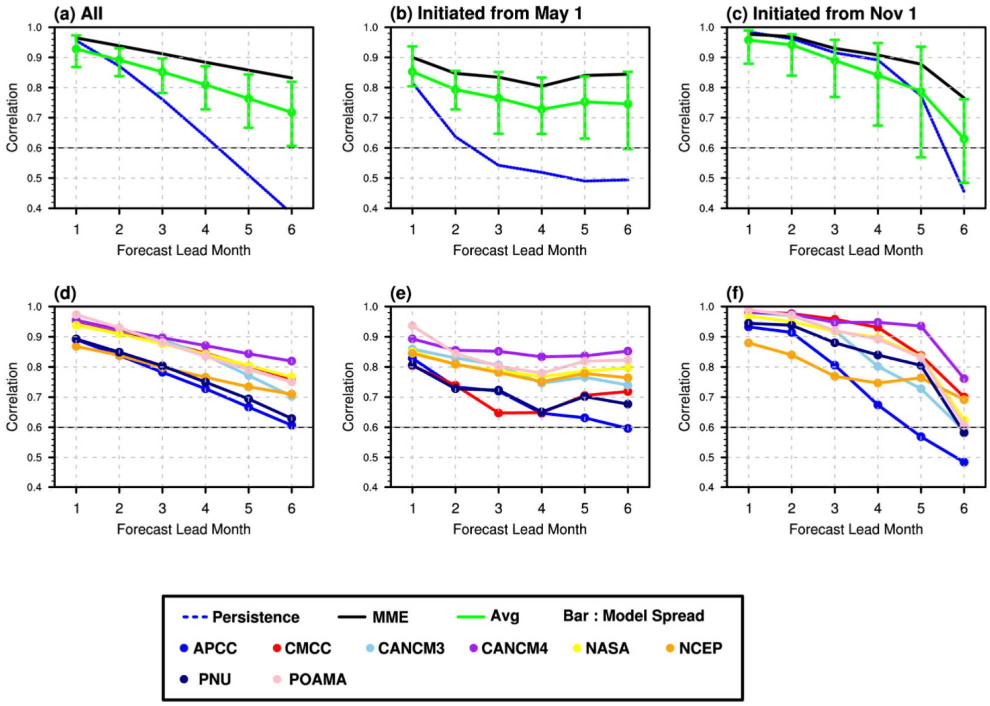


Figure 11 Temporal correlation coefficient (TCC) skills of the prediction of the Niño3.4 sea surface temperature (SST) index as a function of the forecast lead time for (a, d) all seasons combined and the seasons initiated from (b, d) May and (c, f) November. (a, b, c) The blue dashed and black solid lines indicate the skill of the persistent and multi-model ensemble (MME) forecasts, respectively. The averaged skills (solid dot) and ranges (bar) of the individual models (highlighted lines in Figs d, e, and f) are also shown (green). The dotted line indicates the relative reference value of 0.6 for comparison.

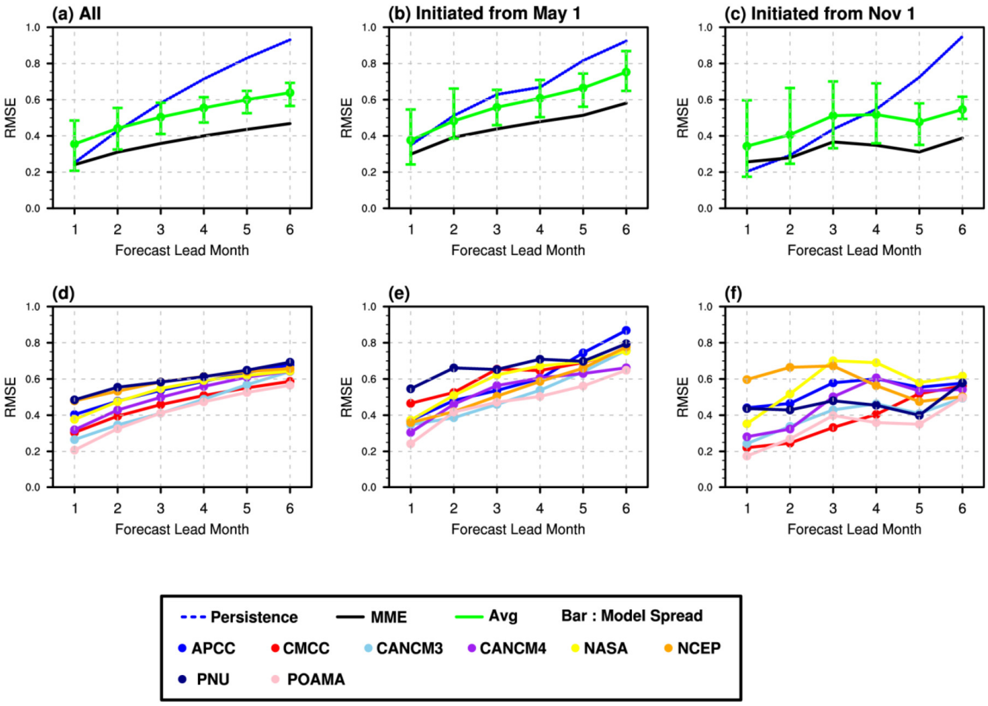


Figure 12 Same as Figure 11 but for the root-mean-square errors.

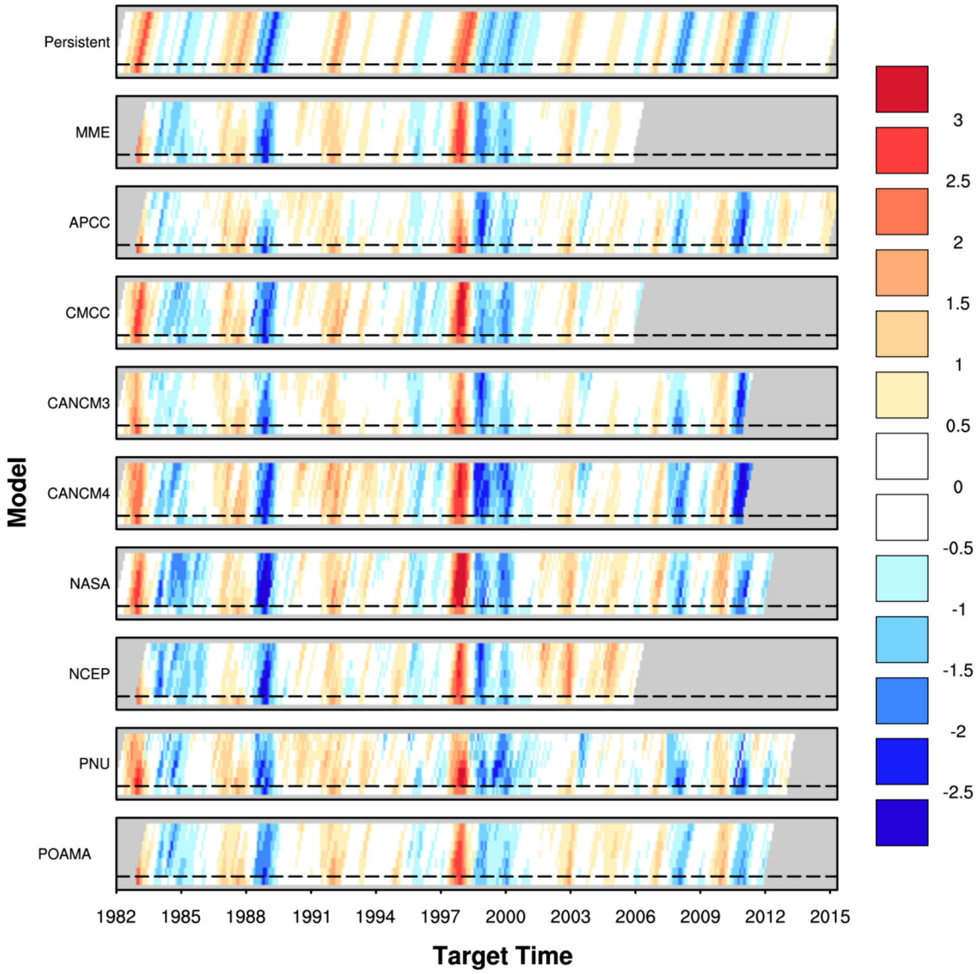


Figure 13　Time series of the monthly mean Niño3.4 index from the observations (bottom rows beneath the dotted lines) and one-to-six month lead times model simulations (y-axis) as a function of the targeted forecast time (x-axis). Each panel highlights one model. The gray shading indicates missing data.

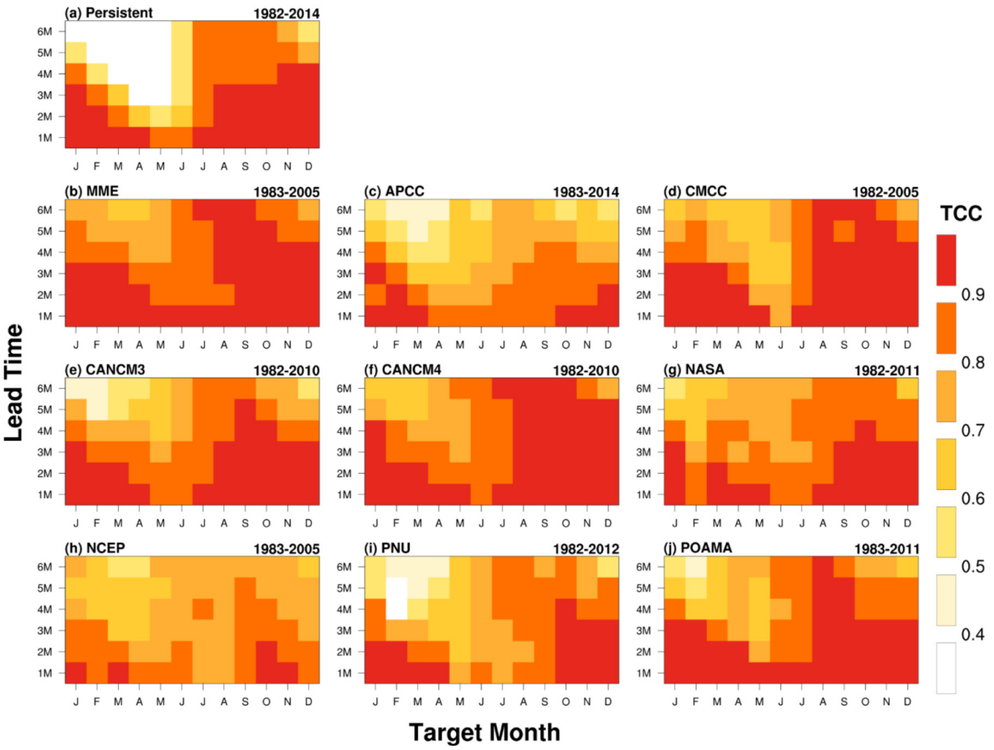


Figure 14 Temporal correlation coefficient (TCC) skills of the prediction of the Niño3.4 index as a function of the targeted forecast time and forecast lead time for (a) persistence, (b) multi-model ensemble (MME), (c) APCC, (d) CMCC, (e) MSC CGCM3, (f) MSC CGCM4, (g) NASA, (f) NCEP, (i) PNU, and (i) POAMA.

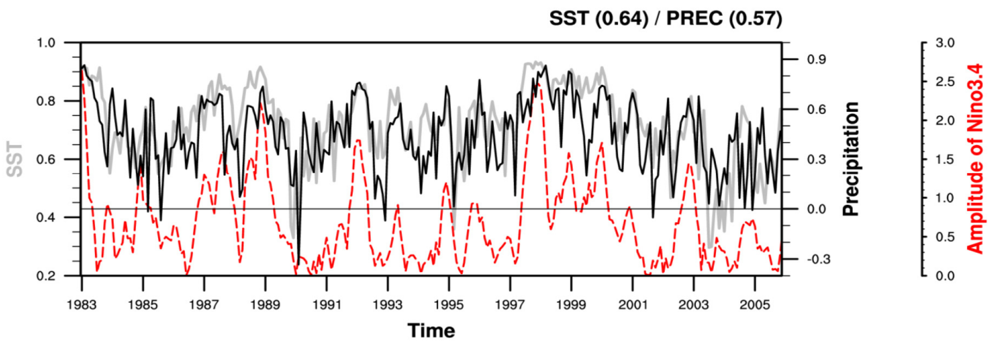


Figure 15 Time series of the observed amplitude of the monthly mean Niño3.4 index (red dashed line) and anomaly pattern correlation (ACC) skill of the tropical Pacific sea surface temperature (SST; grey) and precipitation (black) multi-model ensemble (MME) predictions. The temporal correlation coefficient (TCC) skill between the observed Niño3.4 index and SST (precipitation) prediction skill is given in parentheses in the upper right corner.

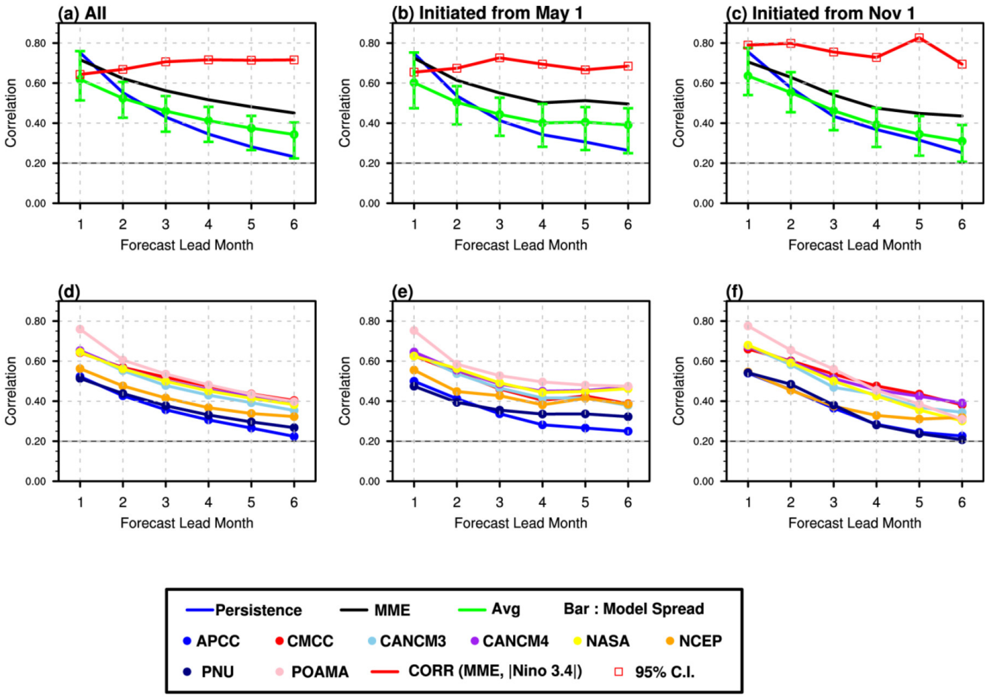


Figure 16 Anomaly pattern correlation (ACC) skills of the prediction of the tropical Pacific sea surface temperature (SST) anomalies as a function of forecast lead times for (a, d) all seasons combined and the seasons initiated from (b, d) May and (c, f) November. (a, b, c) The blue dashed and black solid lines indicate the skill of the persistent and MME forecasts, respectively. The averaged skills (solid dot) and ranges (bar) of the individual models (highlighted lines in Figs 16d, e, and f) are also shown (green). The correlation between the observed amplitude of the Niño3.4 index and SST multi-model ensemble (MME) prediction skill is given (red), where the value at a 5%-significance level is denoted as red square. The dotted line indicates the relative reference value of 0.2.

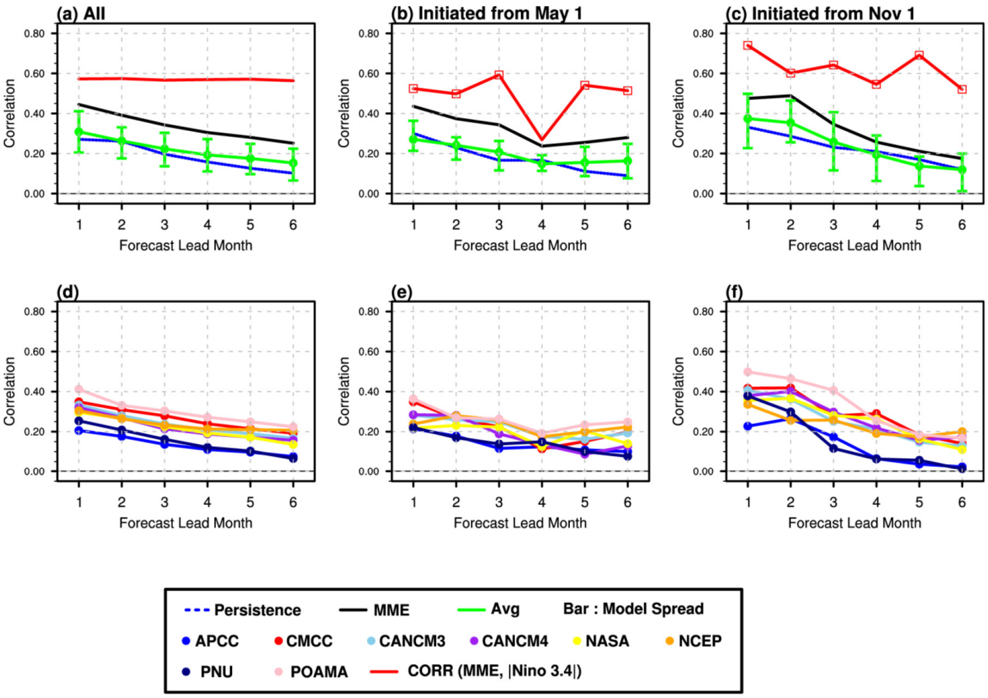


Figure 17 Same as Figure 16 but for precipitation. The dotted line indicates the relative reference value of 0.0.

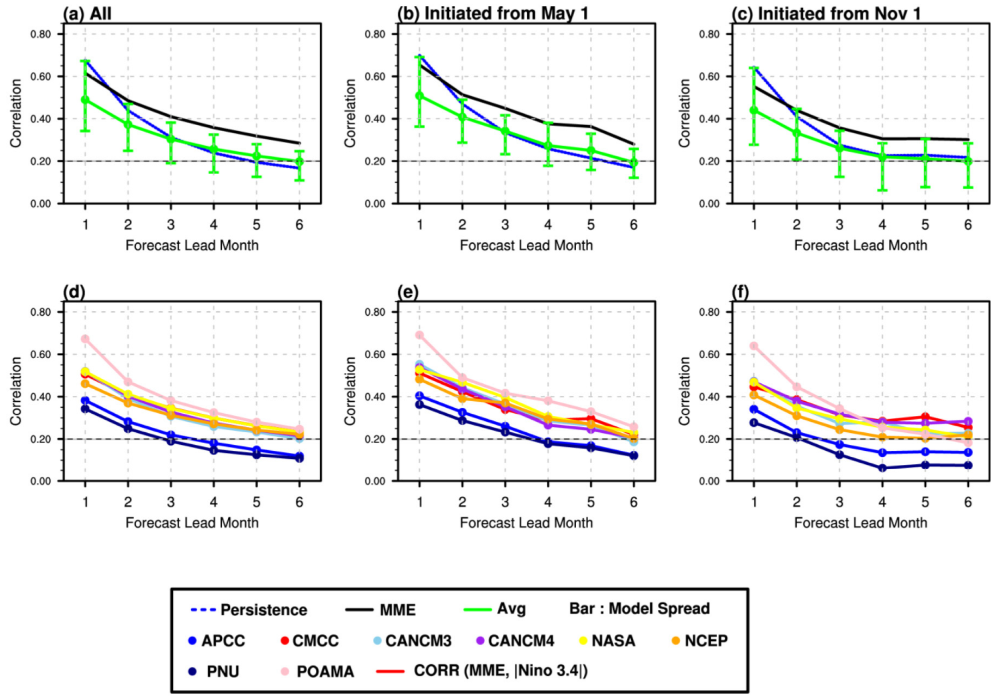


Figure 18 Same as Figure 16 but for the sea surface temperature (SST) diversities. The dotted line indicates the relative reference value of 0.2.

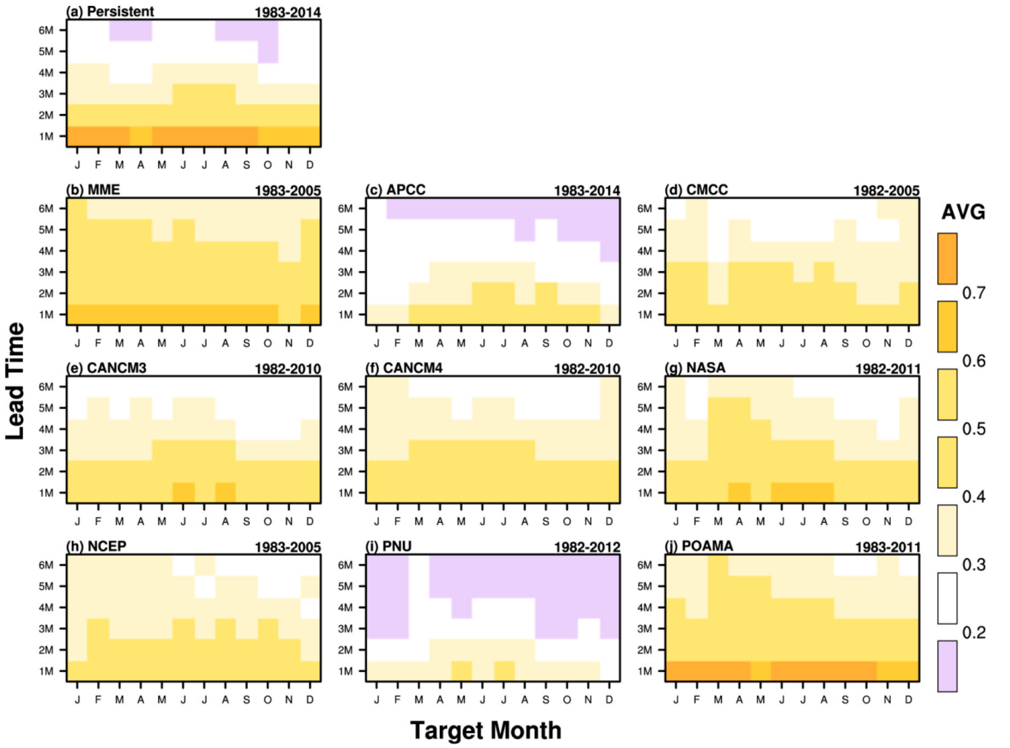


Figure 19 Anomaly pattern correlation (ACC) skills of the sea surface temperature (SST) prediction related to the El Niño-Southern Oscillation (ENSO) diversities as a function of the targeted forecast time and forecast lead times for (a) persistence, (b) multi-model ensemble (MME), (c) APCC, (d) CMCC, (e) MSC CGCM3, (f)MSC CGCM4, (g) NASA, (f) NCEP, (i) PNU, and (i) POAMA.

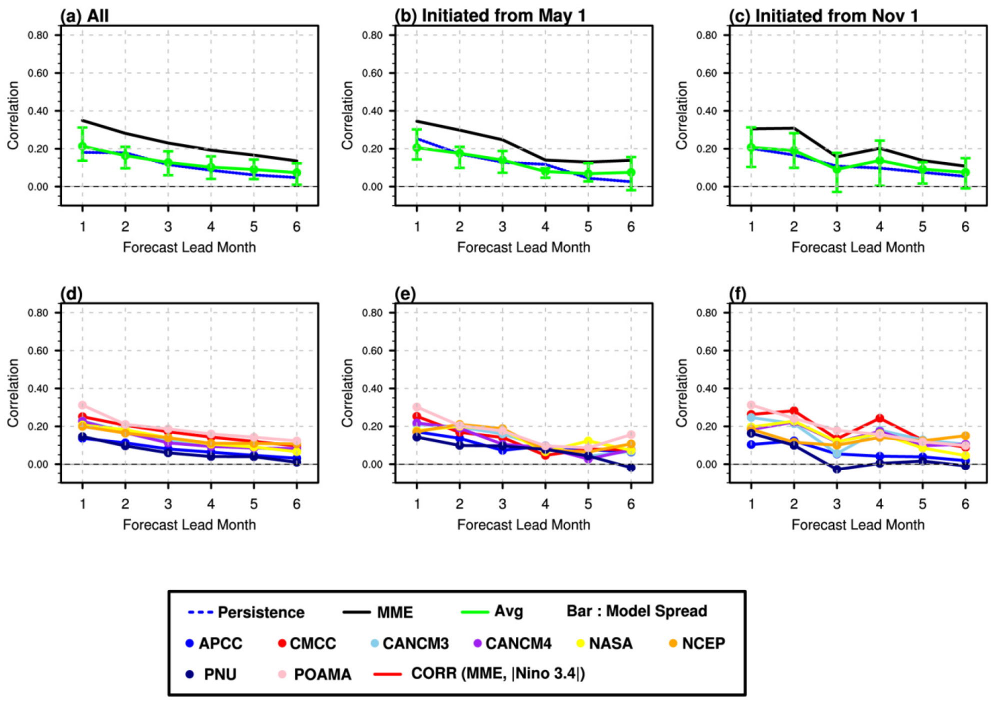


Figure 20 Same as Figure 18 but for the precipitation diversities. The dotted line indicates the relative reference value of 0.0.

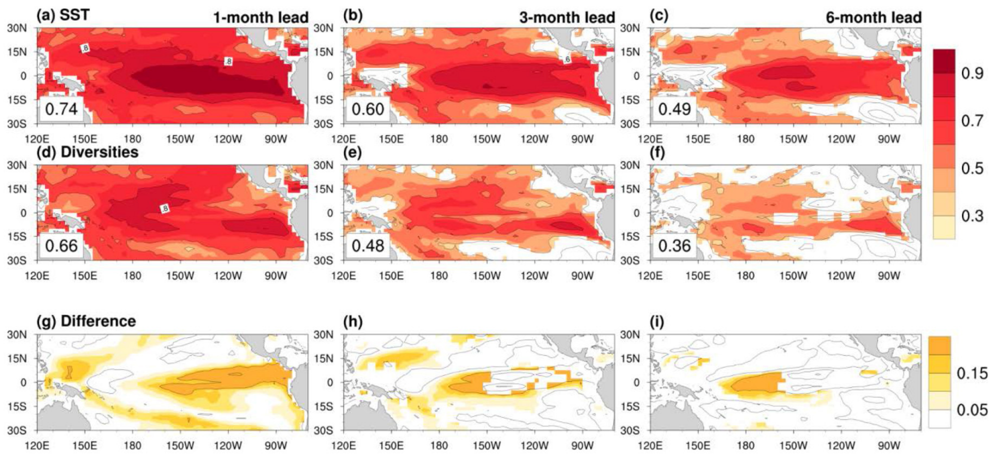


Figure 21 Temporal correlation coefficient (TCC) skills between the observed and multi-model ensemble (MME) monthly mean (a, b, c) SST anomalies and (d, e, f) diversities taken from the whole period from 1983 to 2005 for (a, d) one-, (b, e) three-, and (c, f) six-month lead times. The area-averaged TCC skills are provided in the bottom left of the panels of (a) to (f). The differences between the sea surface temperature (SST) and diversities are also given in Figures 21g, h, and I.

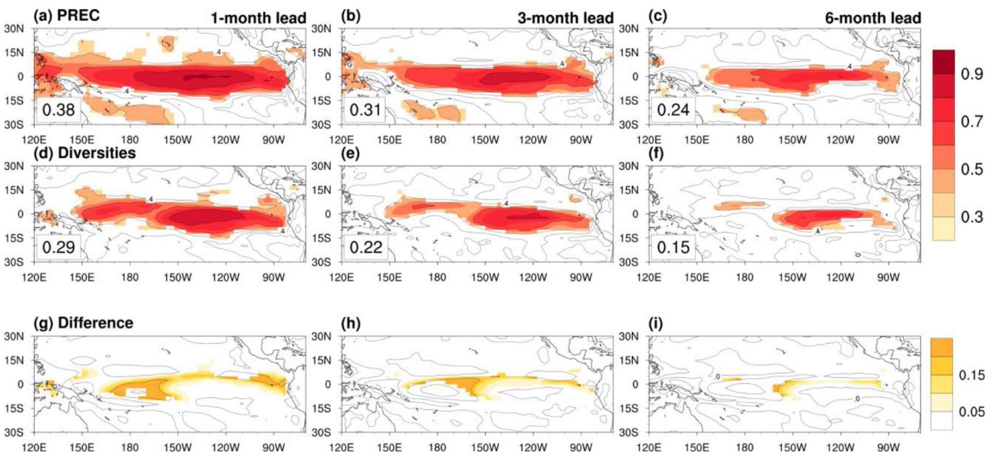


Figure 22 Same as Figure 21 but for precipitation.

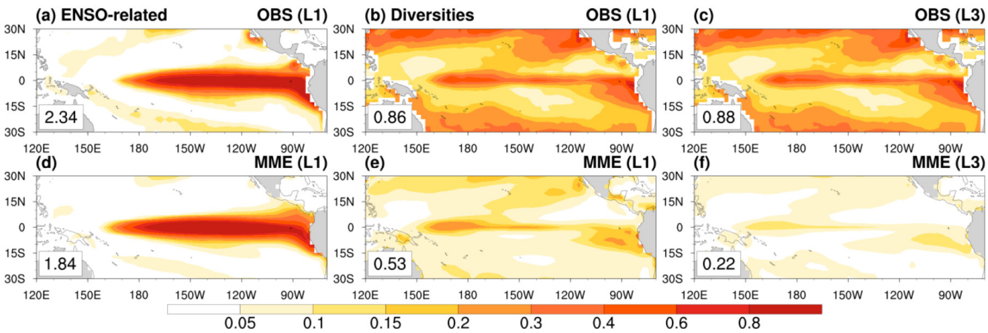


Figure 23 Variance of (a, b, c) the observed and (d, e, f) multi-model ensemble (MME) monthly mean anomalies for the whole period from 1983 to 2005 for the (a, d) El Niño-Southern Oscillation (ENSO)-related variability and diversities for (b, e) one- and (c, f) three-month lead times. The local maximum of the variance is provided in the bottom left of the panels (a-f).

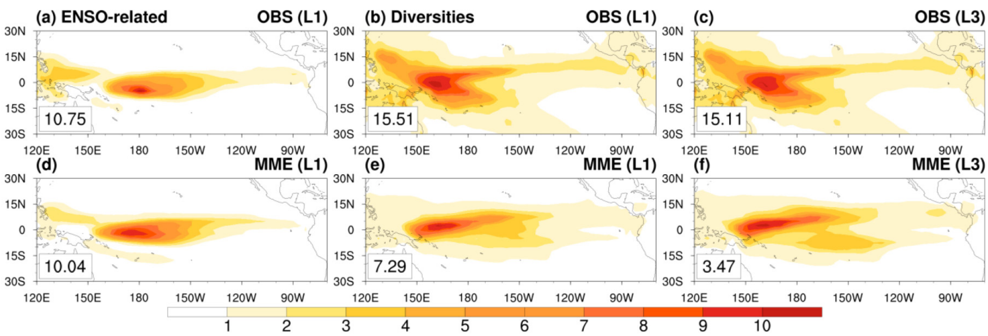


Figure 24 Same as Figure 23 but for precipitation.

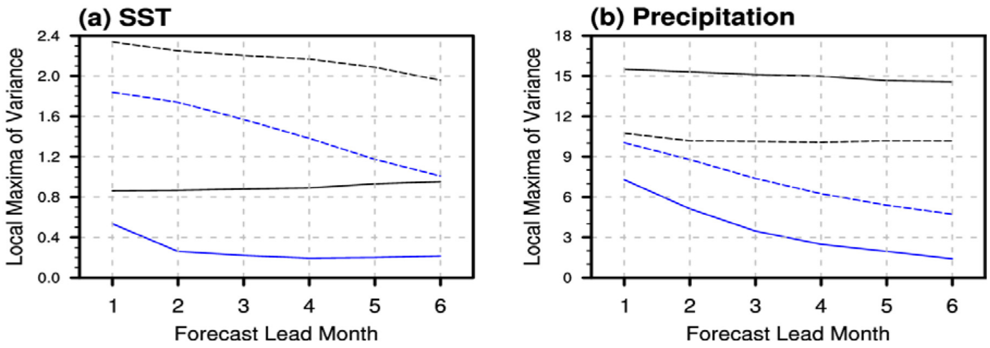


Figure 25 Local maximum of the variance of the observed (black) and multi-model ensemble (MME)-simulated (blue) (a) sea surface temperature (SST) and (b) precipitation variability related to the El Niño-Southern Oscillation (ENSO; dashed lines) and diversities (solid line) as a function of the forecast lead time.

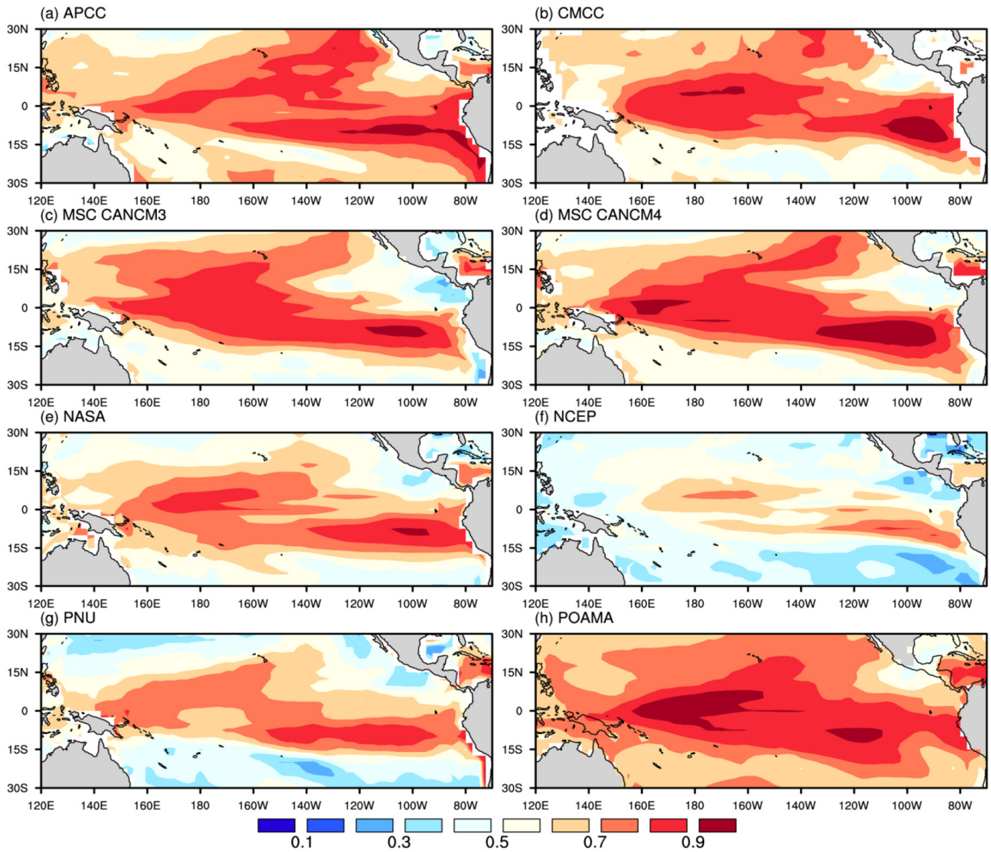


Figure 26 Potential predictability (PP) of the model monthly mean sea surface temperature (SST) diversities for (a) APCC, (b) CMCC, (c) MSC CGCM3, (d) MSC CGCM4, (e) NASA, (f) NCEP, (g) PNU, and (h) POAMA.

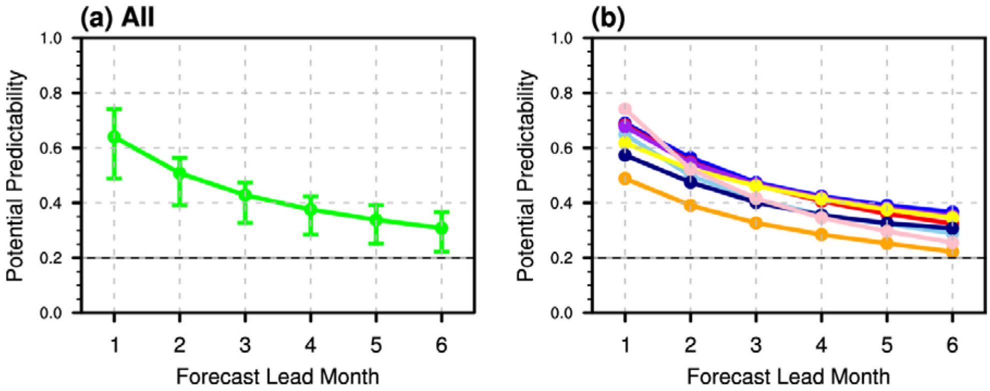


Figure 27 Area-averaged potential predictability (PP) of the sea surface temperature (SST) variability related to the El Niño–Southern Oscillation (ENSO) diversities as a function of the lead time for (a) the average values and ranges of the (b) individual models (see Figure 11 for the relevant legends). The dotted line indicates the relative reference value of 0.2.

APPENDIX

## A1. Climate variability and circulation characteristics of the classified El Niño-Southern Oscillation occurrences

The precipitation changes and circulation characteristics of the classified El Niño-Southern Oscillation (ENSO) occurrences for the boreal warm and cold seasons are presented in Figures A1 and A2. The eastern tropical Pacific receives surplus rainfall during strong El Niño years, with deficit rainfall in the tropical western Pacific and equatorial South America. During weak El Niño years, statistically significant surplus rainfall anomalies were observed in the central equatorial Pacific region, bounded on both sides by the negative rainfall anomalies in the equatorial western and eastern Pacific. In the East Asian region, southern Japan suffers from droughts during weak El Niño years due to the Pacific-Japan pattern (Nitta 1987; Kosaka and Nakamura 2006). During a strong El Niño in the cold season, positive rainfall anomalies were observed over the ITCZ in the eastern and central Pacific, bounded in the west by a broad horseshoe-shaped negative rainfall anomaly centered in the western tropical Pacific that extends eastward into the northern and southern Pacific. Strong winter monsoon rainfall over East Asia, below normal rainfall over Australia, anomalously wet conditions across the southern USA, and anomalously dry conditions over South America were observed. The center of the wet anomalies is located close to the date line in weak El Niño years.

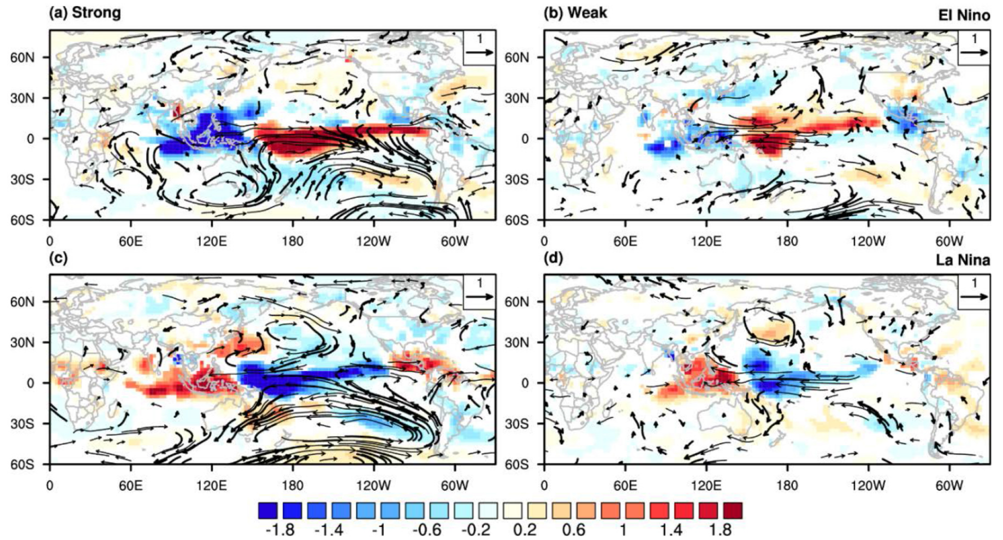


**Figure A1** Composite maps of the anomalous precipitation (shading, see scale at the bottom; units: mm/day) and 850-hPa wind (arrows, see scale in the upper right corner of each panel; units: m/s) during (a, b) El Niño and (c, d) La Niña phases corresponding to (a, c) strong and (b, d) weak El Niño-Southern Oscillation (ENSO) events in the boreal warm season. Shading and arrows denote the precipitation and wind anomalies exceeding the 95% significance level, respectively.

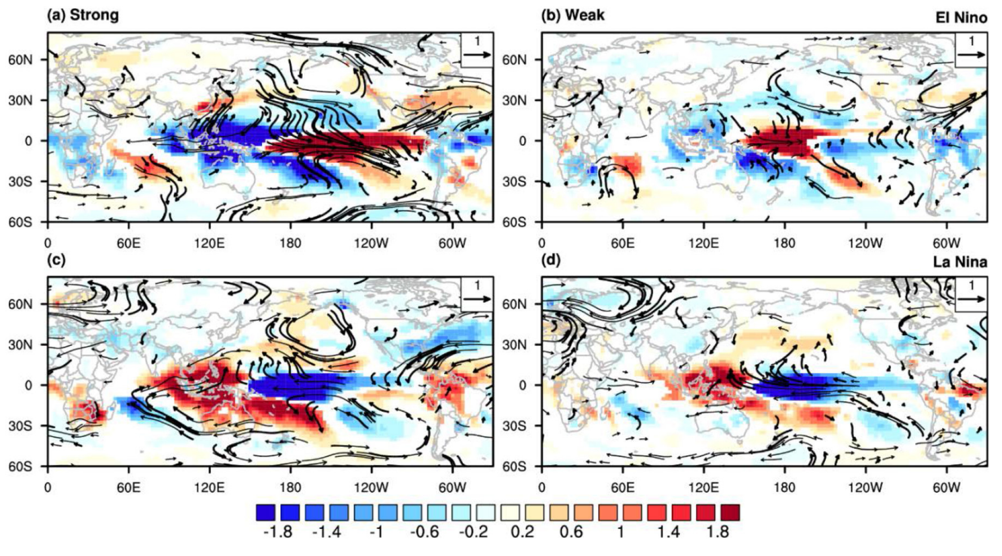


**Figure A2** Same as Figure A1 but for the boreal cold season.

Research Report 2016-11

## Diagnostics of the multi-model ensemble seasonal forecast of the APEC Climate Center: Forecast skill and predictability of ENSO and its response

Soo-Jin Sohn

APEC Climate Center
12 Centum 7-ro, Haeundae-gu, Busan 48058, Republic of Korea
Tel: +82-51-745-3900 Fax: +82-51-745-3949

www.apcc21.org

ISBN 979-11-5698-162-6